ORTA DOĞU TEKNİK ÜNİVERSİTESİ
FEN BİLİMLERİ ENSTİTÜSÜ MÜDÜRLÜĞÜ

TEZ ŞABLONU ONAY FORMU
THESIS TEMPLATE CONFIRMATION FORM

1. Şablonda verilen yerleşim ve boşluklar değiştirilmemelidir.
2. **Jüri tarihi** Başlık Sayfası, İmza Sayfası, Abstract ve Öz'de ilgili yerlere yazılmalıdır.
3. İmza sayfasında jüri üyelerinin unvanları doğru olarak yazılmalıdır. Tüm imzalar **mavi pilot kalemle** atılmalıdır.
4. **Disiplinlerarası** programlarda görevlendirilen öğretim üyeleri için jüri üyeleri kısmında tam zamanlı olarak çalıştıkları anabilim dalı başkanlığının ismi yazılmalıdır. Örneğin: bir öğretim üyesi Biyoteknoloji programında görev yapıyor ve biyoloji bölümünde tam zamanlı çalışıyorsa, İmza sayfasına biyoloji bölümü yazılmalıdır. İstisnai olarak, disiplinler arası program başkanı ve tez danışmanı için disiplinlerarası program adı yazılmalıdır.
5. Tezin **son sayfasının sayfa** numarası Abstract ve Öz'de ilgili yerlere yazılmalıdır.
6. Bütün chapterlar, referanslar, ekler ve CV sağ sayfada başlamalıdır. Bunun için **kesmeler** kullanılmıştır. **Kesmelerin kayması** fazladan boş sayfaların oluşmasına sebep olabilir. Bu gibi durumlarda paragraf (¶) işaretine tıklayarak kesmeleri görünür hale getirin ve yerlerini **kontrol edin**.
7. Figürler ve tablolar kenar boşluklarına taşmamalıdır.
8. Şablonda yorum olarak eklenen uyarılar dikkatle okunmalı ve uygulanmalıdır.
9. Tez yazdırılmadan önce PDF olarak kaydedilmelidir. Şablonda yorum olarak eklenen uyarılar PDF dokümanında yer almamalıdır.
10. Tez taslaklarının kontrol işlemleri tamamlandığında, bu durum öğrencilere METU uzantılı öğrenci e-posta adresleri aracılığıyla duyurulacaktır.
11. Tez yazım süreci ile ilgili herhangi bir sıkıntı yaşarsanız, [Sıkça Sorulan Sorular (SSS)] sayfamızı ziyaret ederek yaşadığınız sıkıntıyla ilgili bir çözüm bulabilirsiniz.

1. Do not change the spacing and placement in the template.
2. Write **defense date** to the related places given on Title page, Approval page, Abstract and Öz.
3. Write the titles of the examining committee members correctly on Approval Page. **Blue ink** must be used for all signatures.
4. For faculty members working in **interdisciplinary programs**, the name of the department that they work full-time should be written on the Approval page. For example, if a faculty member staffs in the biotechnology program and works full-time in the biology department, the department of biology should be written on the approval page. Exceptionally, for the interdisciplinary program chair and your thesis supervisor, the interdisciplinary program name should be written.
5. Write **the page number of the last page** in the related places given on Abstract and Öz pages.
6. All chapters, references, appendices and CV must be started on the right page. **Section Breaks** were used for this. **Change in the placement** of section breaks can result in extra blank pages. In such cases, make the section breaks visible by clicking paragraph (¶) mark and **check their position.**
7. All figures and tables must be given inside the page. Nothing must appear in the margins.
8. All the warnings given on the comments section through the thesis template must be read and applied.
9. Save your thesis as pdf and Disable all the comments before taking the printout.
10. This will be announced to the students via their METU students e-mail addresses when the control of the thesis drafts has been completed.
11. If you have any problems with the thesis writing process, you may visit our [Frequently Asked Questions (FAQ)] page and find a solution to your problem.

☒ **Yukarıda bulunan tüm maddeleri okudum, anladım ve kabul ediyorum. / I have read, understand and accept all of the items above.**

Name : Emre
Surname : Gümüşsu
E-Mail : emre.gumussu@metu.edu.tr
Date : 25/08/2023
Signature : ______________________

NUMERICAL SIMULATION OF HEAT FLOW WITH PARTICIPATING MEDIA RADIATION USING TOTAL ENERGY BASED ENTROPIC LATTICE BOLTZMANN METHOD

A THESIS SUBMITTED TO
THE GRADUATE SCHOOL OF NATURAL AND APPLIED SCIENCES
OF
MIDDLE EAST TECHNICAL UNIVERSITY

BY

EMRE GÜMÜŞSU

IN PARTIAL FULFILLMENT OF THE REQUIREMENTS
FOR
THE DEGREE OF DOCTOR OF PHILOSOPHY
IN
MECHANICAL ENGINEERING

AUGUST 2023

Approval of the thesis:

NUMERICAL SIMULATION OF HEAT FLOW WITH PARTICIPATING MEDIA RADIATION USING TOTAL ENERGY BASED ENTROPIC LATTICE BOLTZMANN METHOD

submitted by **EMRE GÜMÜŞSU** in partial fulfillment of the requirements for the degree of **Doctor of Philosophy in Mechanical Engineering, Middle East Technical University** by,

Prof. Dr. Halil Kalıpçılar
Dean, Graduate School of **Natural and Applied Sciences** _________________

Prof. Dr. M. A. Sahir Arıkan
Head of the Department, **Mechanical Engineering, METU** _________________

Prof. Dr. Hakan I. Tarman
Supervisor, **Mechanical Engineering, METU** _________________

Examining Committee Members:

Prof. Dr. Cüneyt Sert
Mechanical Engineering, METU _________________

Prof. Dr. Hakan I. Tarman
Mechanical Engineering, METU _________________

Prof. Dr. Yusuf Özyörük
Aerospace Engineering, METU _________________

Assoc. Prof. Dr. Özgür Ekici
Mechanical Engineering, Hacettepe University _________________

Assist. Prof. Dr. Onur Baş
Mechanical Engineering, TEDU _________________

Date: 25.08.2023

I hereby declare that all information in this document has been obtained and presented in accordance with academic rules and ethical conduct. I also declare that, as required by these rules and conduct, I have fully cited and referenced all material and results that are not original to this work.

Name Last name : Emre Gümüşsu

Signature :

ABSTRACT

NUMERICAL SIMULATION OF HEAT FLOW WITH PARTICIPATING MEDIA RADIATION USING TOTAL ENERGY BASED ENTROPIC LATTICE BOLTZMANN METHOD

Gümüşsu, Emre
Doctor of Philosophy, Mechanical Engineering
Supervisor : Prof. Dr. Hakan Işık Tarman

August 2023, 93 pages

Operating temperatures of industrial systems are increasing due to requirements for higher efficiency and superior performance. Participating media radiation becomes essential for accurate thermal modeling of these systems. Problems with participating media radiation require solution of all modes of heat transfer. Lattice Boltzmann method emerges as a powerful technique for solution of multi-mode heat transfer problems. The thesis proposes a specific method to implement total energy based formulation of double population entropic lattice Boltzmann method in multi-mode heat transfer problems with participating media. All parameters in the problem are calculated through an integrated lattice Boltzmann solver. Total energy based formulation is modifed to be implemented in these kinds of problems. Chapman Enskog formulation is used for verification of the modification. Reference cases are selected from literature and adopted for validation. Then, duct flow in a participating media is analyzed in a detailed manner. Thereby, a clear explanation is provided for the interaction of flow field with respect to different values of Reynolds number, single scattering albedo and extinction coefficient.

Keywords: Participating media, double population LBM, duct flow, total energy.

ÖZ

IŞINIMA KATILAN ORTAMDA ISI AKIŞININ TOPLAM ENERJİ FORMÜLÜNE DAYALI ENTROPİK KAFES BOLTZMANN YÖNTEMİ İLE ÇÖZÜMÜ

Gümüşsu, Emre
Doktora, Makina Mühendisliği
Tez Yöneticisi: Prof. Dr. Hakan I. Tarman

Ağustos 2023, 93 sayfa

Endüstriyel sistemlerin çalışma sıcaklıkları, yüksek başarım seviyesi ve verimlilik isterleri nedeniyle artış göstermektedir. Bu sistemlerin, kesinlik düzeyi yüksek ısıl benzetimlerinin yapılabilmesi için ışınıma katılan ortamın çözülmesi gerekmektedir. Kafes Boltzmann yöntemi, çok yönlü ısıl akışkan problemlerin çözümünde güçlü bir teknik olmaya başlamıştır. Bu tez kapsamında, toplam enerji formülüne dayanan, entropik kafes Boltzmann yöntemi, ışınıma katılan ortamda çoklu ısı aktarımı problemlerini çözebilmek için geliştirilmiştir. Yöntem üzerinde yapılan değişiklikler, Chapman – Enskog açılımı ile kanıtlanmıştır. Literatürden alınan örnek analizler ile de geliştirilen yöntemin doğrulaması yapılmıştır. Ardından, ışınıma katılan ortam içerisinde, boru içi akış problemi detaylı bir şekilde çözülmüştür. Bu sayede, akış alanının çeşitli değişkenlerle etkileşimi, farklı Reynolds sayısı, tek elektron saçılım beyazlığı ve sönüm katsayısı üzerinden incelenmiştir.

Anahtar Kelimeler: Işınıma Katılan Ortam, çift popülasyonlu kafes Bolztmann yöntemi, kanal içi akış, toplam enerji

Dedicated to my family

ACKNOWLEDGMENTS

I wish to express my deepest gratitude to my supervisor Prof. Dr. Hakan I. Tarman for his continuous support and guidance with his immense knowledge. I never hesitate to ask questions. I always received response to these questions even outside of working hours.

I am grateful to members of thesis monitoring committee, Prof. Dr. Cüneyt Sert and Assoc. Prof. Dr. Özgür Ekici for their contribution throughout the entire study.

I would like to thank Prof. Dr. Yusuf Özyörük and Assist. Prof. Dr. Onur Baş due to their participation in the thesis defense committee.

I have also special thanks to Prof. Dr. Murat Köksal and Assoc. Prof. Dr. Özgür Ekici due to their priceless presence in my academic survey from the beginning.

I would like to thank my managers Ersin Aydın Tekbaş and Mehmet Bahadır Ayata for their contribution to my career and their support.

I am grateful to my friends and colleagues, Efe Can Dağlı, Burak Orhan Günay, Burak Ocak and Çağatay Çelikkaya for their unreserved friendship.

My family also deserves a special thanks due to their tolerance in difficult periods of the thesis and their unconditional love. I get rid of any kind of stress thanks to positive energy of my nephew and niece.

TABLE OF CONTENTS

LIST OF TABLES

TABLES

LIST OF FIGURES

FIGURES

LIST OF ABBREVIATIONS

BC	Boundary Condition
Eq	Equation
FVM	Finite Volume Method
LBM	Lattice Boltzmann Method
Re	Reynolds Number
Ref	Reference
RTE	Radiative Transfer Equation
RTLBM	Radiative Transfer Lattice Boltzmann Method

LIST OF SYMBOLS

α, β	Directional Index
β_{ext}	Extinction Coefficient (1/m)
c	Speed of sound (m/s)
$c_{i,\alpha}$	Directional Lattice Velocity
c_s	Lattice Speed of sound
ϵ	Perturbation Parameter (Knudsen Number)
i	Lattice Velocity Index, Directional Index
t	Time (s)
σ_s	Scattering coefficient (1/m)
σ_a	Absorption coefficient (1/m)
σ	Stefan Boltzmann Constant ($W/m^2/K^4$)
Ω	Solid Angle (str)
Ω'	Solid Angle of the Incoming Radiation (str)
θ	Scattering Phase Function
φ	Single Scattering Albedo
$\delta_{\alpha\beta}$	Kronecker Delta
D	Dimension
L_α	Number of lattices in α direction
P	Pressure (Pa)
ρ	Density (kg/m^3)
ρ_0	Lattice Density
T	Temperature (K)
T_{ref}	Reference temperature for lattice Boltzmann method
U	Velocity (m/s)
μ	Dynamic Viscosity (kg/ms)
δ	Polar Angle
ζ	Azimuthal Angle
k	Thermal Conductivity (W/mK)
ν	Kinematic Viscosity (m^2/s)
H	Duct Height
$\vec{r}, x$	Position of the molecule in LBM

Note: Metric or lattice units are implemented with respect to the equation under consideration.

CHAPTER 1

INTRODUCTION

Fluid flow with participating media radiation is important especially for state of the art industrial systems. The continuous need for increased power leads to the development of systems operating at higher temperatures. Industrial furnaces, combustion chambers, jets and rocket engines are examples for such systems [1]. This trend has substantial impact also on propulsion systems in aviation. Requirements for higher thrust, power and electiricity end up with opeating temperatures almost at the limit of materials.

High temperature levels fundamentally changed procedures of propulsion systems for their design, production, operation and integration. These procedures required comprehensive thermal engineering to have an applicable product. Considering the operating temperatures of these systems and relevant fluid flow such as ventilation, combustion, by-pass, etc., the inclusion of participating media radiation mode of heat transfer is essential for accurate thermal engineering.

Participating media radiation is a complex phenomenon. As in each mode of heat transfer, it is dependent on spatial and temporal variations. However, it contains three additional independent parameters due to its directional (polar and azimuthal) and spectral dependence [1]. Participating media radiation arises from presence of hot gases. Therefore, it usually exists with other modes of heat transfer. Also regarding directional and spectral dependence, participating media radiation is the most complicated and time consuming part of a thermal flow computational model. Such a model should contain numerical solutions of mass, momentum, energy and participating media radiation model equations. Thereby, an integrated model is required to handle fluid flow problems with participating media radiation.

Novel methods are necessary to model participating media problems. Lattice Boltzmann method (LBM) is an evolving technique widely used for flow problems.

Its adoption to thermal problems is an active research area. It can deliver important capabilities in the solution of thermal problems with participating media. It provides results in mesoscopic and macroscopic levels. This can be used in some problems demanding detailed numerical solutions at particle level to obtain macroscopic parameter values. It has a local calculation procedure which allows for an efficient parallelization during the recursions. Parallelization and efficient use of the computational resources are features becoming essential for the current and future implementations of CFD, as computational models are being more complicated, and higher resolution requirements are becoming the essence of having accurate solutions. LBM approaches the computational problem in a transient manner. Thereby, along with an efficient parallelization it can be employed for detailed transient numerical simulation of complex industrial systems.

Main purpose of the thesis is to create an integrated solver using LBM that is capable of numerically simulating multi-mode heat transfer with participating media radiation. The integrated solver involves model equations for mass, momentum, energy and participating media radiation discretized by the total energy based entropic LBM that uses double population for individually representing the momentum and the energy variables.

1.1 Literature Review

LBM evolved for solution of thermal problems, after its successful use for pure flow problems. In order to adapt it for modelling thermal problems, researchers have been developing various techniques. These techniques can be groupped under two main categories: Multi-speed and Double Population techniques. The multi-speed technique is developed simply in order to extend the algebraic precision of LBM. This technique employs lattice structures with more velocity directions. Thereby, it can handle solution of higher order moments required for calculation of energy. In this technique, flow field calculations are fully coupled with the energy calculations. Although it is a natural extension of LBM, it is rarely used in literature to model thermal-flow problems. It suffers from stability issues, complicated boundary treatment and higher computational time. Stability issues are critical that limits the simulation range of the technique. McNamara et al. [2] suggested a method to improve stability using Lax – Wendroff scheme. The same paper also discussed adopting quasi – equilibrium function to define viscosity and thermal diffusivity independent from each other. Much research appeared in literature concentrating on lattice theory and its relation to stability and accuracy of the model. LBM replaces the continuous velocity field with discrete velocities. This procedure is also called velocity space discretization and ends up with lattice structures specific to LBM. Shan et al. [3] clearly showed that velocity discretization at Hermite quadrature nodes corresponds to truncation of equilibrium distribution function to a specific degree in Hermite series expansion. Thereby, a systematic approach can be employed to construct lattices and to have enough physical resolution. There have been various papers using this approach to systematically derive lattice structures [4–6]. Moreover, such a systematic approach also enables handling stability issues better and higher computational efficiency for the required level of physical resolution [4, 7, 8]. Entropic formulation is also applied in the multi-speed technique [7] to sustain stable simulations over wide range of Reynolds numbers (Re). However, none of these improvements manage to fully resolve issues regarding the practical use of multi-speed technique. Stability range is still limited compared to other techniques, and use of larger velocity sets create complexity in boundary treatment [8–10]. In addition, such kind of lattice structures involve higher computational time.

As an alternative, double population technique is used in LBM for thermal problems. Having seperated the treatment of the flow variables and the associated modelling equations, the model enhanced flexibility of LBM. It increases stability and provides solutions with variable Prandtl number (Pr). Drawbacks of this technique are mainly related to its macroscopic correspondence. Flow field and thermal calculations are one way coupled in double population technique. Different formulations exist in the technique. Bartoloni et al. [11] published the first paper for double population technique. They represented temperature as a passive scalar asuming that temperature field doesn’t have any impact on the velocity field. This approach lacks compressibility and viscous heating effects. He and Doolen [12] introduced internal energy formulation. This formulation contains compressibility and viscous heating with specific source terms. However, source terms involve gradients of macroscopic variables. This prevents locality which is critical for LBM to enable efficient parallelization. Total energy formulation was developed by Guo et al. [13] and Karlin et al. [8] to deal with these issues. This formulation is capable of solving full Navier – Stokes equations by including compression work and viscous heating inherently [14]. Thereby, the technique preserves locality of LBM. It is modified for entropic LBM increasing its potential for use in high speed flows [8]. The formulation is also improved for fully coupled analyses of flow field and thermal calculations [15], thus eliminating one of major drawbacks of double population technique.

There are various studies in literature for modeling thermal problems with participating media. Most of these studies use legacy techniques to solve fluid flow and participating media radiation. Some earlier researches employed LBM only for solution of flow field in participating media problems. Calculation of participating media radiation is performed through different techniques such as DOM (Discrete Ordinates Method), CDM (Collapsed Dimension Method) or FVM (Finite Volume Method) [16–19]. Asinari et al. [1] published the first paper for widespread use of LBM in participating media radiation. Later, various papers were published for conduction and radiation problems [20–22]. Many studies [23–26] investigated natural convection in cavity using LBM. In recent years, duct flow with participating media attracted attention due to its correspondence in industrial applications [27, 28]. McCulloch and Bindra [27] adopted LBM for a specific duct problem with porous burner.

All of papers mentioned above adopt passive scalar approach for their models. An integrated model is required to simulate problems with wider range of flow physics. Due to its advantages and potential, this thesis develops a method to adopt total energy based lattice Boltzmann formulation for thermal problems with participating media radiation. The thesis first investigates multi-speed and double population techniques seperately for their potential in the integrated solver. Adopting both techniques require modification of their formulation. Relevant chapters discuss methods for modification of both techniques. Consequently, the suitable technique is selected and implemented for the integrated model. The integration method is verified through Chapman Enskog procedure. Validation procedure includes comparison with reference cases. Once the model is verified and validated, duct flow with participating media is investigated in terms of different solution parameters and their contribution to the result.

Next chapter introduces the problem in terms of its physical and mathematical structure. Chapter 2 is related to fundamentals and implementation of LBM in computationally modelling thermal flows. Participating media radiation and its solution through LBM is also explained in this chapter. Chapter 3 gives detailed information about the integration of different techniques for thermal flow problem with participating media. It also covers verification process. Chapter 4 presents results of the model for validation cases and the case of duct flow with participating media.

1.2 The Problem

Presence of participating media radiation together with the other modes of heat transfer involves more complex physics in comparison to pure conduction, pure convection or pure radiation. Intensity of radiation depends on the temperature distribution in space for radiation emission. Temperature distribution is affected by the flow field and the radiation of the media involved. Therefore, the temperature field is physically coupled with the radiation intensity field as a result of the interaction between radiation and thermal energy.

The flow is considered to take place in a 2D-spatial domain occupied by a viscous fluid. Conservation of mass accounts for total change in density ρ due to transient and convective effects by the flow field $\vec{U}$:

$$\frac{\partial \rho}{\partial t} + \nabla . \left(\rho \vec{U}\right) = 0. \quad (1)$$

Conservation of momentum leads to a balance between total change in momentum of the fluid and the forces due to gravitational acceleration g along the direction, $\vec{X}$,the viscosity and the pressure p:

$$\rho\left(\frac{\partial U_i}{\partial t} + U_j \frac{\partial U_i}{\partial x_j}\right) = \rho g X_i - \frac{\partial p}{\partial x_i} + \frac{\partial}{\partial x_j}\left(\mu\left(\frac{\partial U_i}{\partial x_j} + \frac{\partial U_j}{\partial x_i}\right) + \lambda \frac{\partial U_k}{\partial x_k}\delta_{ij}\right), \quad (2)$$

$i, j = 1,2.$

Conservation of energy accounts for the transient and convective change in thermal energy due to diffusion, dissipation of mechanical energy into thermal energy represented by Φ and the heat source in the form of divergence of radiative heat transfer, $\nabla \cdot q_r$, thus incorporating the effects of the participating media:

$$\rho c_p \frac{\partial T}{\partial t} + \vec{U} \cdot \nabla T = \nabla . (k \nabla T) + \Phi - \nabla \cdot q_r, \quad (3)$$

where

$$\nabla \cdot q_r = 4\pi\sigma_a \left[I_b(\vec{r}, t) - \frac{1}{4\pi}\int_0^{4\pi} I\left(\vec{r}, \vec{\Omega}, t\right) d\vec{\Omega}\right]. \quad (4)$$

Here, I_b denotes the blackbody intensity obtained through the temperature distribution in the domain, $I_b = (\sigma T^4)/\pi$ at the position $\vec{r}$. Integral term is incident radiation, $G(\vec{r},t)$. Radiative transfer equation is solved for radiative intensity I:

$$\frac{1}{c}\frac{\partial I\left(\vec{r}, \vec{\Omega}, t\right)}{\partial t} + \vec{\Omega} \cdot \nabla I\left(\vec{r}, \vec{\Omega}, t\right) = -\sigma_a I\left(\vec{r}, \vec{\Omega}, t\right) - \sigma_s I\left(\vec{r}, \vec{\Omega}, t\right)$$
$$+ \sigma_a I_b(\vec{r}, t) + \sigma_s \oint_0^{4\pi} I\left(\vec{r}, \vec{\Omega}, t\right) \theta\left(\vec{\Omega}', \vec{\Omega}\right) d\Omega. \quad (5)$$

Radiative transfer equation provides mathematical expression for the balance between change in radiative intensity due to losses and gains represented by absorption, $\sigma_a I$, and out-scattering $\sigma_s I$, in-scattering, $\sigma_s \oint_0^{4\pi} I\left(\vec{r}, \vec{\Omega}', t\right) \theta\left(\vec{\Omega}', \vec{\Omega}\right) d\vec{\Omega}'$, and emission, $\sigma_a I_b$. Radiative transfer equation includes three more independent parameters than other modes of heat transfer [1]. The two of them stand for directional dependence $\vec{\Omega}$ and one is for spectral dependence that is not accounted for in this work.

Radiative energy can be augmented or attenuated in the medium during propagation. Both mechanisms form a balance for radiative energy transfer in a participating media [29].

Attenuation decreases radiative energy in its propagation path. Loss of radiative energy is proportional with the extinction coefficient, β_{ext}. Extinction coefficient contains effect of absorption, σ_a, and scattering coefficients, σ_s. Absorption converts radiative energy into the internal energy. Therefore, it causes loss of radiative energy along the path of propagation.

Scattering changes direction of radiative energy. Although it doesn't convert the form of radiative energy, it changes the balance [29]. If scattering directs radiative energy from the direction of interest into other directions, it causes loss of radiative energy in the propagation path [29].

Radiative energy gain is due to emission and in-scattering in participating media. All particles with a finite temperature value emit radiative energy [29]. This emission increases radiative intensity during propagation. On the other hand, scattering can direct radiation from different directions into the direction of propagation. This is called as in-scattering and increases radiative energy in the direction of interest [29].

1.3 Lattice Boltzmann Method

At the heart of Lattice Boltzmann method (LBM) lies the probability distribution function $f(\vec{r},\vec{v},t)$ that gives the probability of finding a molecule at position $\vec{r}$ with a velocity $\vec{v}$ at a time t or the expected number of particles $f(\vec{r},\vec{v},t)d\vec{x}d\vec{v}$ in a phase space volume element $d\vec{r}d\vec{v}$ [30]. The distribution function is connected to macroscopic variables such as the mass density

$$\rho(\vec{r},t) = \int f(\vec{r},\vec{v},t)\, d\vec{v}, \tag{6}$$

the momentum density

$$\rho(\vec{r},t)\vec{u}(\vec{r},t) = \int \vec{v}\, f(\vec{r},\vec{v},t)\, d\vec{v}, \tag{7}$$

and the total energy density

$$\rho(\vec{r},t)E(\vec{r},t) = \frac{1}{2}\int |\vec{v}|^2\, f(\vec{r},\vec{v},t)\, d\vec{v}. \tag{8}$$

These are actually moment integrals of f weighted with some functions of $\vec{v}$ and integrated over the velocity space. The considerations of the internal energy due to the random motion of the particles lead to the macroscopic internal energy density as the moment

$$\rho(\vec{r},t)e(\vec{r},t) = \frac{1}{2}\int |\vec{v}-\vec{u}|^2\, f(\vec{r},\vec{v},t)\, d\vec{v}. \tag{9}$$

Here, $\vec{c} = \vec{v} - \vec{u}$ is the relative (intrinsic) particle velocities in a gas around the mean velocity $\vec{u}$**.** In the presence of an external force $\vec{F}$, the particles in this distribution will be accelerated by $\vec{a}$. If we follow the movements of particles in a phase space volume element during a time interval dt, the number of particles is conserved, thus

$$f(\vec{r}+\vec{v}dt, \vec{v}+\vec{a}dt, t+dt)d\vec{r}d\vec{v} = f(\vec{r},\vec{v},t)d\vec{x}d\vec{v}. \tag{10}$$

The intermolecular collisions taking place within a gas, however, cause changes to the distribution whose effect is summed up by the collision operator $C(f)$ leading to a more realistic equation:

$$f(\vec{r}+\vec{v}dt, \vec{v}+\vec{a}dt, t+dt)d\vec{r}d\vec{v} - f(\vec{r},\vec{v},t)d\vec{r}d\vec{v} = C(f)d\vec{r}d\vec{v}dt. \tag{11}$$

In the limit $dt \to 0$, it reduces to the classical Boltzmann equation [31]:

$$\frac{\partial f}{\partial t} + \vec{v} \cdot \vec{\nabla}_{\vec{r}} f + \vec{a} \cdot \vec{\nabla}_{\vec{v}} f = C(f). \tag{12}$$

The last two terms on the left-hand side of Eq. (12) represent the net number of particles entering the infinitesimal phase-space volume $d\vec{r}d\vec{v}$ centered at $(\vec{r}, \vec{v})$ as the result of inertial motion of particles between collisions and the external force $\vec{F}$**,** respectively, while the term on the right-hand side represents the net number of particles entering that same volume as the result of instantaneous and purely local collisions. The collision operator must fulfil the conservation of the mass

$$\int C(f) d\vec{v} = 0.. \tag{13}$$

the total momentum

$$\int \vec{v}\, C(f) d\vec{v} = 0. \tag{14}$$

and the total energy conditions

$$\int \vec{v} \cdot \vec{v}\, C(f) d\vec{v} = 0. \tag{15}$$

due to the assumption that the collisions do not create nor destroy molecules. The general Boltzmann collision operator is rather complicated, and the collision operator used in the LBM is based on much simpler BGK collision operator [32]

$$C_{BGK}(f) = -\frac{f - f^{eq}}{\tau}. \tag{16}$$

where τ is the relaxation parameter towards the equilibrium (Maxwellian) distribution

$$f^{eq} = \rho \left(\frac{1}{2\pi RT}\right)^{3/2} exp\left(-\frac{|\vec{v} - \vec{u}|^2}{2RT}\right). \tag{17}$$

with the specific gas constant R and density ρ. The relaxation parameter τ is closely related to the viscosity ν. BGK collision operator satisfies the conservation requirements Eqs. (13)-(15) and facilitates the evolution of f towards f^{eq} as governed by the relaxation parameter τ.

Boltzmann showed that the functional

$$\mathcal{H} = \int f \ln f \, d\vec{v}. \tag{18}$$

reaches its minimum value when the distribution function f reaches equilibrium f^{eq}. Thus, if the molecules are distributed in some other way, then the value of $\mathcal{H}$ will be higher. It can be shown directly from the Boltzmann equation Eq. (12) that $\mathcal{H}$ is not conserved in the system, it never increases, but instead it decreases, until the particle distribution reaches equilibrium [33]. This is called the Boltzmann H-theorem. It states that molecular collisions invariably drive the distribution function towards equilibrium. It can be considered a necessary criterion for any collision operator in kinetic theory. This is, in fact, satisfied by the BGK collision operator. H-theorem is considered analogous to how the thermodynamic quantity of entropy always increases in a system unless the system has reached an equilibrium characterized by an entropy maximum. Thus, $\mathcal{H}$ is also referred to as entropy function.

The Boltzmann equation is a continuous equation, and it is necessary to construct corresponding discrete equations for computational modelling. The first step in the discretization process involves the discretization of the moment equations Eqs. (13)-(15) in the velocity space:

$$\int f(\vec{r}, \vec{v}, t) \, d\vec{v} \cong \sum_{\alpha} \varpi_\alpha f(\vec{r}, \vec{v}_\alpha, t), \tag{19}$$

$$\int \vec{v} \, f(\vec{r}, \vec{v}, t) \, d\vec{v} \cong \sum_{\alpha} \varpi_\alpha \vec{v}_\alpha f(\vec{r}, \vec{v}_\alpha, t), \tag{20}$$

$$\tfrac{1}{2}\int |\vec{v}|^2\, f(\vec{r},\vec{v},t)\, d\vec{v} \cong \frac{1}{2}\sum_{\alpha} \varpi_\alpha |\vec{v}_\alpha|^2 f(\vec{r},\vec{v}_\alpha,t), \tag{21}$$

where $\{\vec{v}_\alpha\}$ is a discrete set of velocities and ϖ_α are the corresponding weights. This is introduced into the Boltzmann equation Eq. (12) with the BGK collision operator Eq. (16) to get (BGK-Boltzmann)

$$\frac{\partial f_\alpha}{\partial t} + \vec{v}_\alpha \cdot \nabla_{\vec{x}} f_\alpha = -\tfrac{1}{\tau}(f_\alpha - f_\alpha^{eq}). \tag{22}$$

where $f_\alpha = f(\vec{r},\vec{v}_\alpha,t)$ and the external force is omitted. This decouples the velocity space and the physical space, and the resulting equation is called the continuous Lattice Boltzmann Equation (LBE). Discretization of Eq. (23) in space and time with finite difference formulas leads to the (discrete) Lattice Boltzmann Equation:

$$f_\alpha(\vec{r} + \vec{v}_\alpha \Delta t, t + \Delta t) - f_\alpha(\vec{r},t) = -\tfrac{\Delta t}{\tau}(f_\alpha(\vec{r},t) - f_\alpha^{eq}(\vec{r},t)). \tag{23}$$

This form is widely used as a computational tool for the simulation of fluid flow. The evolution of the distribution function is approximated over a lattice having each lattice site located at $\vec{r}$ and connected to the neighbouring lattice sites along the directions $\vec{v}_\alpha$. The implementation takes successive streaming (propagation) and collision (relaxation) sub-steps.

The high accuracy evaluation of the integrals in discrete form based on the Gauss-Hermite quadrature that is based on the Hermite polynomials

$$H^{(n)}(r) = \frac{(-1)^n}{\omega(r)} \frac{d^n}{dx^n} \omega(r). \tag{24}$$

for integer $n \geq 0$ where $\omega(r)$ is the weight function

$$\omega(r) = \frac{1}{\sqrt{2\pi}} \exp(-r^2/2). \tag{25}$$

that are orthogonal under a weighted inner product

$$\int_{-\infty}^{\infty} H^{(n)}(r)H^{(m)}(r)\,\omega(r)dr = n!\,\delta_{nm}. \tag{26}$$

Note that the form of the equilibrium (Maxwellian) distribution in Eq. (17) facilitates the use of the Hermite polynomials that are orthogonal with respect to the Gaussian weight function $\omega(r)$.

Yet another consideration in deriving the lattice configurations is physical, the isotropy of the lattice [34]. Sufficiency of isotropy in the lattice configuration depends on the underlying physics of the model. The isotropy considerations lead to the following conditions:

$$\begin{aligned}
&\textstyle\sum_\alpha w_\alpha = 1,\\
&\textstyle\sum_\alpha w_\alpha \vec{v}_{\alpha,i} = 0,\\
&\textstyle\sum_\alpha w_\alpha \vec{v}_{\alpha,i}\vec{v}_{\alpha,j} = \delta_{ij},\\
&\textstyle\sum_\alpha w_\alpha \vec{v}_{\alpha,i}\vec{v}_{\alpha,j}\vec{v}_{\alpha,k} = 0,\\
&\textstyle\sum_\alpha w_\alpha \vec{v}_{\alpha,i}\vec{v}_{\alpha,j}\vec{v}_{\alpha,k}\vec{v}_{\alpha,m} = \left(\delta_{ij}\delta_{km} + \delta_{ik}\delta_{jm} + \delta_{im}\delta_{jk}\right),\\
&\textstyle\sum_\alpha w_\alpha \vec{v}_{\alpha,i}\vec{v}_{\alpha,j}\vec{v}_{\alpha,k}\vec{v}_{\alpha,m}\vec{v}_{\alpha,n} = 0.
\end{aligned} \tag{27}$$

together with the weights w_α to be non-negative. In order to simulate advection-diffusion problems, for example, lower level of isotropy may be sufficient.

The main distinction of the entropic LBM is in the way of constructing f_α^{eq} in the (discrete) LBE, Eq. (25), that it requires and enforces f_α^{eq} to minimize the discrete form of the functional $\mathcal{H}$. As stated by the H-theorem, it is a necessary criterion. This has been shown to be effective in stabilizing LBM in contrast the classical construction of f_α^{eq} that is solely based on moment-matching only.

CHAPTER 2

LATTICE BOLTZMANN METHOD

Previous chapter introduces physics and mathematical structure of the main problem. Fluid flow with participating media requires solution of mass, momentum, energy and participating media radiation. Thereby, an integrated model should contain equations for each conserved property. This chapter describes LBM for solving each conservation equation. It contains fundamental information about modeling techniques used throughout the thesis.

2.1 Calculation of Mass, Momentum and Energy

The techniques for the numerical solutions of mass and momentum equations using LBM are quite established in literature. Further considerations of the energy equation requires substantial change in the mathematical structure of the method. There are two techniques to perform calculations for energy. These are the multi-speed and the double population techniques. This chapter explains both techniques. Their fundamentals are demonstrated along with the underlying differences.

2.1.1 Multi-Speed Lattice Boltzmann Method

Multi – speed technique is a natural extension of LBM [14]. Alexander et al. [35] introduced this technique to perform thermal calculations using LBM. Multi-speed technique utilizes the following discrete equation to calculate flow field,

$$f_i(\vec{r} + \mathrm{c_i}\Delta t, t + \Delta t) - f_i(\vec{r}, t) = -\frac{\Delta t}{\tau^*}(f_i(\vec{r}, t) - f_i^{eq}(\vec{r}, t)) \qquad (28)$$

where τ^* is relaxation time, and it depends on dynamic viscosity [36]:

$$\mu = \frac{2}{D}\rho e\left(\tau^* - \frac{1}{2}\right).$$

The technique achieves macroscopic properties through moments of probability distribution function, $f_i(\vec{r},t)$. Multispeed technique requires fourth order moments to fully resolve Navier Stokes equations [36]. While zeroth and first order moments are necessary for mass-momentum calculations,

$$\sum_{i=1}^{N} f_i^{eq} = \sum_{i=1}^{N} f_i = \rho, \qquad \sum_{i=1}^{N} c_{i\alpha} f_i^{eq} = \sum_{i=1}^{N} c_{i\alpha} f_i = \rho u_\alpha,$$

second order moment gives total energy E,

$$\sum_{i=1}^{N} c_{i\alpha} c_{i\beta} f_i^{eq} = \sum_{i=1}^{N} c_{i\alpha} c_{i\beta} f_i = \frac{2}{D}\rho e \delta_{\alpha\beta} + \rho u_\alpha u_\beta,$$

where

$$\rho e = \rho E - \frac{1}{2}\rho|u|^2, \qquad e = \frac{D}{2}T.$$

third and fourth order moments give momentum and energy fluxes.

$$\begin{aligned} \sum_{i=1}^{N} c_{i\alpha} c_{i\beta} c_{i\gamma} f_i^{eq} &= \sum_{i=1}^{N} c_{i\alpha} c_{i\beta} c_{i\gamma} f_i = Q_{\alpha\beta\gamma} \\ \sum_{i=1}^{N} c_{i\alpha} c_{i\beta} c^2 f_i^{eq} &= \sum_{i=1}^{N} c_{i\alpha} c_{i\beta} c^2 f_i = \forall_{\alpha\beta} \end{aligned} \qquad (29)$$

where

$$Q_{\alpha\beta\gamma} = \rho u_\alpha u_\beta u_\gamma + \frac{2}{D}\rho e(u_\alpha \delta_{\beta\gamma} + u_\beta \delta_{\alpha\gamma} + u_\gamma \delta_{\alpha\beta})$$

$$\forall_{\alpha\beta} = \rho \frac{4(D+2)}{D^2} e^2 \delta_{\alpha\beta} + \frac{2}{D}\rho e^2 u^2 \delta_{\alpha\beta} + \frac{2(D+4)}{D}\left(\rho e \mathrm{u}_\alpha \mathrm{u}_\beta + \rho u^2 \mathrm{u}_\alpha \mathrm{u}_\beta\right).$$

Shan et al. [5] and Philippi et al. [4] showed that 9th order algebraic accuracy is necessary to accurately calculate fourth order moment of f_i^{eq}. They also ascertained that the minimum of 37 velocity directions are required to have 9th order algebraic accuracy. Therefore, a model has to adopt D2Q37 lattice to fully resolve Navier – Stokes equations, if it is based on multi-speed technique.

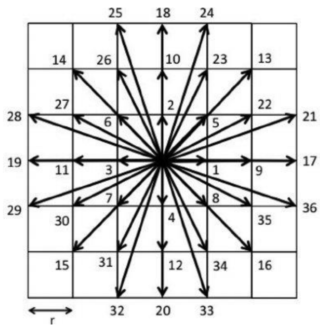

Figure 1: D2Q37 lattice with its discrete velocities. Reprinted from Ref. [37]

Figure 1 demonstrates D2Q37 lattice along with its velocity directions. As seen in the figure, there are multiple velocity sets with different magnitudes. Some directions stretch out to neighboring lattices. Each velocity direction represents an energy shell according to its magnitude. Table 1 lists velocity sets according to their energy shells they reside in. Weights and overall magnitudes of velocity directions are also shown in the table.

Table 1: Energy Levels and Lattice Weights of D2Q37

Energy Level	Velocity Magnitude	Lattice Weight
1	0	0.846393
2	1	0.107306
3	$\sqrt{2}$	5.76679e-2
4	2	1.42082e-2
5	$\sqrt{5}$	5.35305e-3
6	$2\sqrt{2}$	1.01194e-3
7	3	2.45301e-4
8	$\sqrt{10}$	2.83414e-4

The Lattice Boltzmann Equation (LBE), Eq. (28), corresponds to conservation equations through its zeroth, first and second order moments. Table 2 lists order of moment of the LBE and its macroscopic correspondents. As can be seen in table, multi-speed technique is capable of solving whole Navier – Stokes equations.

Table 2: Moments of LBE in Multi-Speed Technique

Mesoscopic Equation	Macroscopic Equation	Order of Moment
Eq. (28)	$\frac{\partial \rho}{\partial t} + \nabla.(\rho U) = 0$	0th
Eq. (28)	$\frac{\partial \rho U}{\partial t} + U.\nabla(\rho U) = -\nabla p + \partial_\alpha\left[\mu\left(\partial_\beta u_\alpha + \partial_\alpha u_\beta\right)\right] + \nabla(\lambda \nabla.U)$	1st
Eq. (28)	$\frac{\partial \rho e}{\partial t} + U.\nabla \rho e = -p\nabla.U + \nabla.(k\nabla e) - \left[\mu\left(\partial_\beta u_\alpha + \partial_\alpha u_\beta\right)\right]\partial_\alpha u_\beta + \lambda(\nabla.U)^2$	2nd

Equilibrium distribution function is different than that of hydrodynamic methods. As mentioned above, order of truncation is of the essence for equilibrium distribution function. According to the truncation or lattice structure, equilibrium distribution function involves terms to a certain degree. Regarding fourth order terms are necessary for calculation of thermal flows, equilibrium distribution function, Eq. (30), is given with fourth order terms [38].

$$
\begin{aligned}
f_i^{eq} = w_i \rho [1 + c_{i\alpha} u_\alpha + \frac{1}{2}[(c_{i\alpha} u_\alpha)^2 - u^2] + \frac{T-1}{2}(c_i^2 - \mathrm{D}) \\
+ \frac{c_{i\alpha} u_\alpha}{6}\left[(c_{i\alpha} u_\alpha)^2 - 3u^2] + \frac{T-1}{2}(c_{i\alpha} u_\alpha)(c_i^2 - \mathrm{D} - 2)\right] \\
+ \frac{1}{24}[(c_{i\alpha} u_\alpha)^4 - 6(c_{i\alpha} u_\alpha)^2 u^2 + 3u^4] \\
+ \frac{T-1}{4}[(c_i^2 - D - 2)[(c_{i\alpha} u_\alpha)^2 - u^2] - 2(c_{i\alpha} u_\alpha)^2] \\
+ \frac{T-1^2}{8}[c_i^4 - 2(D+2)c_i^2 + D(D+2)].
\end{aligned} \quad (30)
$$

Mathematical structure of the equation includes effect of temperature on the collision process [5, 14] contrary to pure hydro-dynamic cases.

2.1.2 Double Population Lattice Boltzmann Method

As introduced earlier, there are two different versions of total energy based LBM. This thesis employs formulation proposed by Karlin et al. [8] as the baseline. As in all double population techniques for heat flow problems, the discretized model governs evolution of two distribution functions f_i and g_i, along characteristic directions $\vec{c_i}$, associated with macroscopic quantities, mass-momentum and energy, respectively:

$$
f_i \, f_i(\vec{r} + \vec{c_i}\,\Delta t, t + \Delta t) - f_i(\vec{r}, t) = -\frac{\Delta t}{\tau^*}\left(f_i(\vec{r}, t) - f_i^{eq}(\vec{r}, t)\right), \quad (31)
$$

$$
g_i(\vec{r} + \vec{c_i}\,\Delta t, t + \Delta t) - g_i(\vec{r}, t) = -\frac{\Delta t}{\tau}\left(g_i(\vec{r}, t) - g_i^{eq}(\vec{r}, t)\right), \quad (32)
$$

where the relaxation times τ^* and τ in each equation are associated with the kinematic viscosity v and thermal conductivity k coefficients as follows:

$$
v = (\tau^* - \frac{\Delta t}{2})T_0, \qquad k = (\tau - \frac{\Delta t}{2})T_0, \qquad T_0 = c_s^2.
$$

The zeroth and first order moments of f_i provide the density and the velocity of the flow field, while the zeroth order moment of g_i provides the total energy as given below:

$$\sum_{i=1}^{N} f_i^{eq} = \sum_{i=1}^{N} f_i = \rho, \qquad \sum_{i=1}^{N} \mathrm{c}_{\mathrm{i}\alpha}\, f_i^{eq} = \sum_{i=1}^{N} \mathrm{c}_{\mathrm{i}\alpha}\, f_i = \rho u_\alpha, \tag{33a}$$

$$\sum_{i=1}^{N} g_i^{eq} = \sum_{i=1}^{N} g_i = 2\rho \mathrm{E} = D\rho \mathrm{T} + \rho u^2, \tag{33b}$$

on a lattice configuration of DdQN. Equilibrium distribution function for the total energy is derived from Grad's method [39]:

$$\mathrm{g_i^{eq}}(\vec{\mathrm{r}},\mathrm{t}) = \mathrm{w_i}\left[2\rho\mathrm{E} + \frac{q_\alpha^{eq}\mathrm{c}_{\mathrm{i}\alpha}}{\mathrm{T}_0} + \frac{R_{\alpha\beta}^{eq} - 2\rho\mathrm{E}\mathrm{T}_0\delta_{\alpha\beta}}{2T_0^2}\left(\mathrm{c}_{\mathrm{i}\alpha}\mathrm{c}_{\mathrm{i}\beta} - \mathrm{T}_0\delta_{\alpha\beta}\right)\right], \tag{34a}$$

where

$$R_{\alpha\beta}^{eq} = 2\rho E\left(T_0\delta_{\alpha\beta} + u_a u_\beta\right) + 2\rho T_0\left(T_0\delta_{\alpha\beta} + 2u_a u_\beta\right), \tag{34b}$$

is contracted fourth order moment flux and

$$q_\alpha^{eq} = 2\rho E u_a + 2\rho T_0 u_a, \tag{34c}$$

is the energy flux. Karlin et al. [8] modified the model with entropic LBM rendering it suitable for high-speed flows due to stability of entropic formulation. Participating media radiation usually exists with high-speed flows in industrial systems such as jet engine plumes or combustion chambers. Therefore, entropic LBM is of preference also in this study to exploit the model capability for high-speed flows in future studies. The equilibrium distribution function f_i^{eq} associated with the entropic LBM for D2Q9 lattice configuration is given in Appendix.

Total energy based double population LBM is applicable with different lattice configurations. This work utilizes D2Q9 lattice configuration considering its computational efficiency and simplicity. This lattice configuration is shown in Figure 2. The associated lattice velocities and weights are listed in Table 3. Speed of sound, c_s, in D2Q9 lattice is $\frac{1}{\sqrt{3}}$.

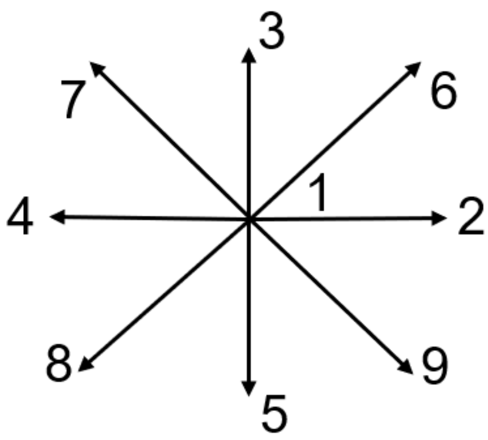

Figure 2: D2Q9 lattice configuration for the discrete mass-momentum and energy models

Table 3: Lattice velocities and weights for D2Q9 lattice.

$\vec{c_i}$	(0,0)	(1,0) (0,1) (−1,0) (0,−1)	(1,1) (−1,1) (−1,−1) (1,−1)
w_i	$\frac{4}{9}$	$\frac{1}{9}$	$\frac{1}{36}$

2.2 Calculation of Participating Media Radiation

As it has achieved a considerable success in heat flow simulations, LBM is further extended to participating media radiation [1]. By exploiting the similarity between Boltzmann equation and radiative transfer equation, several models have been developed for RTLBM [40, 41]. The method proposed by Asinari et al. [1] is based on radiative equilibrium assumption in the domain. It solves an LBE to calculate radiative intensity values I_i along the characteristic directions $\vec{c_i}$ for a gray and homogeneous medium:

$$I_i(\vec{r} + \vec{c_i}\,\Delta t, t + \Delta t) - I_i(\vec{r}, t) = -\,\frac{\Delta t}{\tau_i}\Big(I_i(\vec{r}, t) - I_i^{eq}(\vec{r}, t)\Big), \tag{35}$$

where I_i^{eq} is the equilibrium distribution function having a specific form for participating media radiation:

$$I_i^{eq}(\vec{r}, t) = \sum_{i=1}^{N} I_i w_i. \tag{36}$$

Relaxation time τ_i involves effect of extinction coefficient β_{ext} and lattice dependent velocities $c_{i\alpha}$, and it is given by $\tau_i = 1/(\beta_{ext}\,\|\vec{c_i}\|\,)$ [1].

Participating media radiation is a 3D phenomenon having directional dependence on polar ($0 \leq \delta \leq \pi$) and azimuthal ($0 \leq \zeta \leq 2\pi$) angles. It is transformed into two-dimensional domain by assuming isotropy in polar angle, thus angular dependence of radiative intensity is taken only for azimuthal angle [1]. This is accomplished by properly adjusting lattice configuration and weights [1]. There are several options for a suitable lattice configuration. This work adopts D2Q8 lattice configuration considering simplicity and computational efficiency. The characteristic directions are the same as that of D2Q9, but without the zero velocity as shown in Figure 3. Weights are equal to each other in all directions as listed in Table 4 [1]. Speed of sound is 1 in this lattice configuration [1].

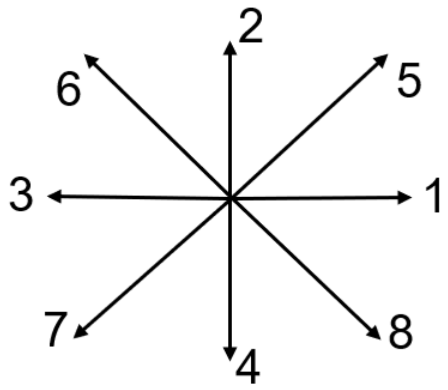

Figure 3: D2Q8 lattice structure for radiation model

Table 4: Velocities and weights for D2Q8 lattice

Velocity	$(1,0)$	$(0,1)$	$(-1,0)$	$(0,-1)$	$(1,1)$	$(-1,1)$	$(-1,-1)$	$(1,-1)$
Weight	$\frac{1}{8}$	$\frac{1}{8}$	$\frac{1}{8}$	$\frac{1}{8}$	$\frac{1}{8}$	$\frac{1}{8}$	$\frac{1}{8}$	$\frac{1}{8}$

The computed radiative intensity values I_i are then used to calculate incident radiation or the integral term in Eq. (4) [21]:

$$G(\vec{r},t) = \sum_{i=1}^{N} I_i w_i \tag{37}$$

which is necessary for the determination of the divergence of radiative heat transfer $\vec{\nabla} \cdot \vec{q}_r$ as defined in Eq. (4).

CHAPTER 3

INTEGRATION OF PARTICIPATING MEDIA SOLUTION INTO THE THERMAL MODEL

Energy equation, Eq. (3), contains divergence of radiative heat transfer, $\nabla \cdot q_r$, as a source to represent effect of participating media radiation. This requires an integration procedure for LBM to correspond to physically proper expressions at macroscopic scale. Integration procedure involves a modification process. Modified equations are verified through Chapman-Enskog procedure. This chapter evaluates both multi-speed and total energy based double population LBM for the integrated model. Then, their potential use in the integrated model is discussed in detail.

3.1 Multi-Speed Technique

The form of the discrete equation that Multi-speed LBM utilizes is given in Eq. (28). The equation corresponds to conservation equations at macroscopic level with its moments at different orders. The technique is able to represent compressiblity effects and viscous heating at macroscopic scale.

Energy problems with heat source requires modification of the basic LBE, namely Eq. (28). Main requirement for the modification is to attain correct equations at macroscopic level. The modification process should be performed so that while energy equation is represented in the correct manner, conservation of mass and momentum correspondence remain as the same at the macroscopic level. In other words, heat source should be properly introduced into the energy equation without affecting the forms of mass and momentum equations.

The modification starts with a source term added to LBE distributing it through lattice weights for each direction:

$$f_i(\vec{r} + \mathrm{c_i}\Delta t, t + \Delta t) - f_i(\vec{r}, t) = -\frac{\Delta t}{\tau^*}\left(f_i(\vec{r}, t) - f_i^{eq}(\vec{r}, t)\right) + \Delta t q_i. \tag{38}$$

Chapman-Enskog expansion is necessary to identify the macroscopic correspondent of the proposed Eq. (28). The expansion is with respect to Knudsen number $\in$ for each lattice direction [33, 35, 42].

$$f_i = f_i^{(0)} + \in f_i^{(1)} + \in^2 f_i^{(2)}$$

$$\partial_t = \in \partial_t^{(1)} + \in^2 \partial_t^{(2)}, \qquad \partial_a = \in \partial_a^{(1)}, \qquad q_i = \in q_i^{(1)}$$

for substitution in Eq. (28). Resultant equation can be divided into groups with respect to order of magnitude of Knudsen number:

$$O(\in^0): \qquad f_i^{(eq)} = f_i^{(0)}, \tag{39a}$$

$$O(\in^1): \qquad \partial_t^{(1)} f_i^{(0)} + c_{ia}\partial_a^{(1)} f_i^{(0)} = -\frac{1}{\tau^*} f_i^{(1)} + q_i^{(1)}, \tag{39b}$$

$$\begin{aligned} O(\in^2): \qquad & \partial_t^{(1)} f_i^{(1)} + \partial_t^{(2)} f_i^{(0)} + c_{ia}\partial_a^{(1)} f_i^{(1)} \\ & + \frac{1}{2} c_{ia} c_{ia} \partial_a^{(1)} \partial_a^{(1)} f_i^{(0)} + c_{ia}\partial_a^{(1)} \partial_t^{(1)} f_i^{(0)} \\ & + \frac{1}{2} \partial_t^{(1)} \partial_t^{(1)} f_i^{(0)} = -\frac{1}{\tau^*} f_i^{(2)}. \end{aligned} \tag{39c}$$

Eq. (39c) can be rearranged using (39b) and manipulated as Eq. (40), [35]:

$$\begin{aligned} O(\in^2): \qquad & \partial_t^{(2)} f_i^{(0)} + \left(1 - \frac{1}{2\tau^*}\right)\left[\partial_t^{(1)} f_i^{(1)} + c_{ia}\partial_a^{(1)} f_i^{(1)}\right] \\ & = -\frac{1}{\tau^*} f_i^{(2)} - \frac{1}{2} c_{ia}\partial_a^{(1)} q_i^{(1)} - \frac{1}{2}\partial_t^{(1)} q_i^{(1)}. \end{aligned} \tag{40}$$

In order to have macroscopic equations for conservation of mass, momentum and energy, moments of Eq. (39b) and Eq. (40) are necessary. Summation of moments of these equations culminate in conservation of mass, momentum and energy equations at zeroth, first and second order as seen in Table 5.

Table 5: Macroscopic counterparts of the LBE in Eq. (38) with respect to different orders of magnitudes

Mesoscopic Equation	Macroscopic Equation
$\sum_{i=1}^{M} Eq.(39b) + \sum_{i=1}^{M} Eq.(40)$	$\frac{\partial \rho}{\partial t} + \nabla.(\rho U) + \forall_1 = 0$
$\sum_{i=1}^{M} c_{ia} Eq.(39b) + \sum_{i=1}^{M} c_{ia} Eq.(40)$	$\frac{\partial \rho U}{\partial t} + U.\nabla(\rho U) = -\nabla p + \partial_\alpha[\mu(\partial_\beta u_\alpha + \partial_\alpha u_\beta)] + \nabla(\lambda \nabla.U) + \forall_2$
$\sum_{i=1}^{M} c_{ia} c_{ia} Eq.(39b) + \sum_{i=1}^{M} c_{ia} c_{ia} Eq.(40)$	$\frac{\partial \rho e}{\partial t} + U.\nabla \rho e = -p\nabla.U + \nabla.(k\nabla e) - [\mu(\partial_\beta u_\alpha + \partial_\alpha u_\beta)]\partial_\alpha u_\beta + \lambda(\nabla.U)^2 + \forall_3$

As shown in Table 5, the proposed equations end up with additional terms represented by, $\forall_1, \forall_2, \forall_3$:

$$\forall_1 = \sum_{i=1}^{M} q_i^{(1)} + \sum_{i=1}^{M} -\frac{1}{2} c_{ia} \partial_a^{(1)} q_i^{(1)} - \frac{1}{2} \partial_t^{(1)} q_i^{(1)}$$

$$\forall_2 = \sum_{i=1}^{M} c_{ia} q_i^{(1)} + \sum_{i=1}^{M} c_{ia} (-\frac{1}{2} c_{ia} \partial_a^{(1)} q_i^{(1)} - \frac{1}{2} \partial_t^{(1)} q_i^{(1)})$$

$$\forall_3 = \sum_{i=1}^{M} c_{ia} c_{ia} q_i^{(1)} + \sum_{i=1}^{M} c_{ia} c_{ia} (-\frac{1}{2} c_{ia} \partial_a^{(1)} q_i^{(1)} - \frac{1}{2} \partial_t^{(1)} q_i^{(1)})$$

These terms contain expressions related to the heat source appearing in Eq. (38) and appear as a result of heat source added to the LBE.

These extra terms are unphysical expressions appearing in mass and momentum equations that need to be eliminated. 2^{nd} order moment also doesn't end up with a clean source term being applicable for macroscopic form of energy conservation equation. Moreover, these terms in all conservation equations are intractable, as they contain spatial and temporal derivatives.

Several methods are investigated to overcome this issue. Options evaluated throughout this thesis are listed below:

- A better use of lattice isotropy,
- Modification of the equilibrium distribution function,
- Accepting these terms in mass and momentum equations,
- A different methodology as in compressible flows or inclusion of body force term,

Lattice isotropy can be used to make residual terms vanishing for some orders of moments. However, a mathematical expression eliminating residual terms couldn't be found in the thesis. Equilibrium distribution function can be modified to compensate residual terms. Such a modification requires comprehensive work in molecular physics. Therefore, it is considered as out of scope of the thesis. Equations can be solved with these residuals to evaluate their impact on the solution accuracy. These terms may be accepted, if resulting error is low. This strategy doesn't converge to a solution, as non-physical results are received in these models. The last item considers use of specific source terms to eliminate residuals. Nevertheless, methods used to contain source terms in momentum calculations don't work for energy sources. Therefore, a suitable source term couldn't be developed. Consequently, studies demonstated that multi-speed LBM technique is not applicable in the thesis study.

3.2 Total Energy Based Double Population Lattice Boltzmann Method

Double population technique has seperate distribution functions and LBE for calculation of mass, momentum and energy. This enables modification of energy equation without affecting mass and momentum equations to include heat source term. Thus, modification is performed only on the second LBE standing for the energy equation. The proposed equation contains heat source term distributed via lattice weights for each lattice direction as in previous section of this chapter:

$$g_i(\vec{r}+\vec{c_i}\Delta t, t+\Delta t) - g_i(\vec{r},t) = -\frac{\Delta t}{\tau}\left(g_i(\vec{r},t) - g_i^{eq}(\vec{r},t)\right) + \Delta t\, q_i, \qquad (41a)$$

where

$$q_i = C_1 w_i Q. \qquad (41b)$$

Here, $Q = -\vec{\nabla}\cdot\vec{q}_r$ is the volumetric source term, q_i is its directional form along the lattice directions and the constant C_1 is used to eliminate any residual terms in the corresponding macroscopic equations. Thus, the proposed modification contains the radiative source term along the lattice directions $\vec{c_i}$ via lattice weights w_i.

For the purpose of obtaining the macroscopic correspondent of the proposed equation, Eq. (41a), a perturbation expansion is performed:

$$g_i = {g_i}^{(0)} + \in {g_i}^{(1)} + \in^2 {g_i}^{(2)}$$

$$\partial_t = \in {\partial_t}^{(1)} + \in^2 {\partial_t}^{(2)}, \qquad \partial_a = \in {\partial_a}^{(1)}, \qquad q_i = \in {q_i}^{(1)}$$

in different orders of the Knudsen number, $\in$. These expansions are substituted into Eq. (41b) and then the terms corresponding to different orders of magnitude are extracted:

$O(\in^0)$: $$g_i{}^{(eq)} = g_i{}^{(0)}, \tag{42a}$$

$O(\in^1)$: $$\partial_t{}^{(1)} g_i{}^{(0)} + c_{ia}\partial_a{}^{(1)} g_i{}^{(0)} = -\frac{1}{\tau} g_i{}^{(1)} + q_i{}^{(1)}, \tag{42b}$$

$O(\in^2)$: $$\begin{aligned}&\left(1-\frac{\Delta t}{2\tau}\right)\left(\partial_t{}^{(1)} + c_{ia}\partial_a{}^{(1)}\right) g_i{}^{(1)} + \partial_t{}^{(2)} g_i{}^{(0)} \\ &+ \frac{\Delta t}{2}\left[\partial_t{}^{(1)} + c_{ia}\partial_a{}^{(1)}\right] q_i{}^{(1)} = -\frac{1}{\tau} g_i{}^{(2)}.\end{aligned} \tag{42c}$$

The sum of the zeroth order moments of equations (42b) and (42c) yield:

$$\begin{aligned}\partial_t T = &-u_a\partial_a T - \frac{2}{D}T_0\partial_a u_a - \frac{2}{D\rho}\Pi_{a\beta}\partial_a u_\beta + \frac{1}{\rho}\partial_a\left(\tau - \frac{\Delta t}{2}\right)\rho T_0 \partial_a T \\ &+ \frac{C_1}{D\rho}Q - \frac{\Delta t}{2}\frac{1}{D\rho}\partial_t C_1 Q\end{aligned} \tag{43}$$

where $\Pi_{a\beta} = -v\rho(\partial_a u_\beta + \partial_\beta u_a)$. It can be seen in Eq. (43) that there appears an extra term in the form of $-\frac{\Delta t}{2}\frac{1}{D\rho}\partial_t C_1 Q$.

In order to eliminate this term, a procedure as proposed by Seta [42] is applied that involves introducing adjustable constants, A and B, in thermal lattice Boltzmann formulations (33b) and (41b):

$$2\rho E = \sum_{i=1}^{N} g_i + A\, C_1 Q, \qquad q_i = w_i Q B C_1. \tag{44}$$

The perturbation procedure is repeated on Eq. (41a), now adopting new parameters A and B. Reorganizing the resulting equation in the orders of magnitudes of ∈ yields:

$$O(\in^1): \qquad \partial_t{}^{(1)}T = -u_a\partial_a{}^{(1)}T - \frac{2}{D}T_0\partial_a{}^{(1)}u_a + \frac{1}{\tau}A\frac{C_1}{D\rho}Q + B\frac{C_1}{D\rho}Q \quad (45a)$$

$$O(\in^2): \qquad \partial_t{}^{(2)}T = -\frac{2}{D\rho}\Pi_{a\beta}\partial_a{}^{(1)}u_\beta + \frac{1}{\rho}\partial_a{}^{(1)}\left(\tau - \frac{\Delta t}{2}\right)\rho T_0\partial_a{}^{(1)}T - \frac{1}{D\rho}\partial_t{}^{(1)}C_1Q\left[\frac{\Delta t}{2\tau}A - A + B\frac{\Delta t}{2\tau}\right] \quad (45b)$$

The constants A and B are adjusted so that no extra term remains in these equations. Thus, for a proper expression for the source term, the constants A and B must satisfy the relations:

$$\frac{1}{\tau}A + B = 1, \qquad A\frac{\Delta t}{2\tau} - A + B\frac{\Delta t}{2\tau} = 0,$$

yielding

$$A = \frac{\Delta t}{2}, \qquad B = 1 - \frac{\Delta t}{2\tau}. \quad (46)$$

These forms given in Eq. (46) are consistent with those proposed in [42]. Thereby, justifying that this procedure is also valid for total energy formulation based double population LBM.

Adopting these expressions for A and B of Eq. (46), in the formulations (33b) and (41b) yields the following form of the energy equation:

$$\partial_t T = -\frac{2}{D\rho}\Pi_{a\beta}\partial_a u_\beta + \frac{1}{\rho}\partial_a\left(\tau - \frac{\Delta t}{2}\right)\rho T_0\partial_a T - u_a\partial_a T - \frac{2}{D}T_0\partial_a u_a + \frac{C_1}{D\rho}Q. \quad (47)$$

This equation suggests that for the model to recover energy equation in the correct form, C_1 should be chosen in the following specific form:

$$C_1 = \frac{D\rho}{c_p\rho_0}$$

The form of C_1 contains model parameters. D is dimension of the spatial domain and ρ stands for lattice density. Denominator contains specific heat under constant pressure, c_p, and fluid density, ρ_0, at macroscopic scale which are equal to unity in the model [8, 33].

3.2.1 Definition of the Heat Source Term in Lattice Dimensions

LBM performs calculations at mesoscopic scale. Moments of the LBE define macroscopic equations in lattice units. Equations and all parameters are calculated according to this specific dimensional system. Participating media radiation is also computed in lattice units, and integration procedure should have a clear representation of the heat source term at macroscopic scale. This requires rearrangement of conservation of energy equation in lattice dimensions.

The macroscopic and dimensional form of energy equation in metric units is given in Eq. (3) in Section 1.2. Unit conversion is performed with respect to parameters defined in lattice units [33]. The quantities in lattice units are indicated with a superscript '*'. The notation is specific to this section of the chapter. In other sections, the quantities are used in lattice units as default. In

$$T = C_T\, T^*, \qquad U = C_u\, U^*, \qquad t = C_t\, t^*, \qquad x = C_x\, x^*, \qquad p = C_p\, p^*,$$
$$\nabla q_r = C_I\, \varphi, \qquad I = C_I\, I^*,$$

T^*, U^*, t^*, x^* and φ are parameters in lattice units, whereas C_T, C_u, C_t, C_x are conversion factors [1, 27, 33]. Here

$$\rho_0^* = 1,\ \Delta x^* = 1,\ \Delta t^* = 1,$$

$$C_T = T_{ref},\ \ C_x = \Delta x = \frac{H}{M},\ \ C_t = \Delta t,\ \ C_\rho = \rho,\ \ C_I = \sigma T_{Ref}^4,$$

C_t is dependent on kinematic viscosity and thermal diffusivity [33]:

$$v = v^* \frac{{C_x}^2}{C_t}, \qquad \alpha = \alpha^* \frac{{C_x}^2}{C_t}, \qquad \alpha^* = \frac{k^*}{\rho_0^* c_p^*}.$$

Remaining parameters can be derived from available conversion factors [33], such as,

$$C_u = \frac{C_x}{C_t}.$$

LBE represents an energy equation which is transformed with respect to above mentioned parameters and conversion factors. Starting from the dimensional form of conservation of energy, the conversion process ends up with the following form of the equation:

$$\frac{C_T}{C_t}\frac{\partial T^*}{\partial t^*} + U^* C_u \frac{C_T}{C_x}\frac{\partial T^*}{\partial x^*} + V^* C_u \frac{C_T}{C_x}\frac{\partial T^*}{\partial y^*} = \frac{k}{\rho c_p}\frac{C_T}{C_x^2}\left(\frac{\partial^2 T^*}{\partial x^{*2}} + \frac{\partial^2 T^*}{\partial y^{*2}}\right) + \frac{1}{c_p}\frac{C_x^2}{C_t^3}\Phi^* - \frac{\sigma T_R^4}{\rho c_p}\varphi, \tag{48}$$

where

$$\varphi = \sigma_a \Theta = \sigma_a \left[4T^{*4} - \int_{\vec{\Omega}=0}^{4\pi} I^*\left(\vec{r}, \vec{\Omega}, t\right) d\vec{\Omega}\right],$$

and so $$\Theta = \left[4T^{*4} - \int_{\vec{\Omega}=0}^{4\pi} I^*\left(\vec{r}, \vec{\Omega}, t\right) d\vec{\Omega}\right].$$

The equation can be rearranged to give,

$$\frac{\partial T^*}{\partial t^*} + U^* \frac{\partial T^*}{\partial x^*} + V^* \frac{\partial T^*}{\partial y^*} = \alpha \frac{C_t}{C_x^2}\left(\frac{\partial^2 T^*}{\partial x^{*2}} + \frac{\partial^2 T^*}{\partial y^{*2}}\right) + \frac{1}{c_p}\frac{C_x^2}{C_t^2 C_T}\Phi^* - \frac{C_t}{C_T}\frac{\sigma T_{Ref}^4 \sigma_a}{\rho c_p}\Theta, \tag{49}$$

with the coefficient,

$$\frac{1}{c_p}\frac{C_x^2}{C_t^2 C_T} = \text{Ч}^*.$$

Substituting expression for α^* into the Eq. (49) gives,

$$\frac{\partial T^*}{\partial t^*} + U^* \frac{\partial T^*}{\partial x^*} + V^* \frac{\partial T^*}{\partial y^*} = \alpha^* (\frac{\partial^2 T^*}{\partial x^{*2}} + \frac{\partial^2 T^*}{\partial y^{*2}}) + Ч^* \Phi^* - \frac{C_t}{C_T} \frac{\sigma T_{Ref}^4 \sigma_a}{\rho c_p} \Theta \quad (50)$$

The last term corresponds to the divergence of radiative heat flux and can be manipulated as:

$$\frac{\partial T^*}{\partial t^*} + U^* \frac{\partial T^*}{\partial x^*} + V^* \frac{\partial T^*}{\partial y^*} = \alpha^* \left(\frac{\partial^2 T^*}{\partial x^{*2}} + \frac{\partial^2 T^*}{\partial y^{*2}} \right) + Ч^* \Phi^* - C_x^2 \alpha^* \frac{\beta_{ext} \sigma_a}{4N} \Theta. \quad (51)$$

Extinction coefficient and absorption coefficient are converted to lattice units [27],

$$\beta_{ext} = C_\beta \beta_{ext}^*, \qquad \sigma_a = C_\beta \sigma_a^*, \qquad C_\beta = \frac{1}{H}.$$

The process results in the energy equation in lattice units with heat source term representing participating media radiation,

$$\frac{\partial T^*}{\partial t^*} + U^* \frac{\partial T^*}{\partial x^*} + V^* \frac{\partial T^*}{\partial y^*} = \alpha^* (\frac{\partial^2 T^*}{\partial x^{*2}} + \frac{\partial^2 T^*}{\partial y^{*2}}) + Ч^* \Phi^* - \frac{1}{M^2} \alpha^* \frac{\beta_{ext}^* \sigma_a^*}{4N} \Theta. \quad (52)$$

Therefore, heat source in the Eq. (47) is equal to:

$$Q = \frac{1}{M^2} k^* \frac{\beta_{ext}^* \sigma_a^*}{4N} \Theta. \quad (53)$$

This form of the heat source should be substituted into the underlying LBE, Eq. (41a), in order to end up with a proper expression solving the correct equation at macroscopic scale.

3.3 Evaluation of Both Methods

LBM has two main techniques to handle thermal flows. In this section, both techniques are evaluated for their use in the integrated model. Multi-speed technique is advantageous due to its intrinsic capability to solve a coupled flow field. The evaluation of energy and flow field are fully coupled with each other. Compressibility effects and viscous heating are also represented in this technique.

Thereby, an integrated model solving mass, momentum, energy and radiation in a fully coupled manner is possible with multi-speed technique. However, the technique has certain drawbacks that impede its widespread use in literature. First, the technique has stability issues. Kinematic viscosity and thermal diffusivity are allowed to vary in a narrow band to ensure a stable solution. This limits the technique to low speed flows. Multi-speed technique depends on algebraic order of accuracy of the lattice structure. Therefore, it requires lattice configurations with larger velocity sets extending towards neighboring lattices. Boundary treatment becomes substantially complicated in these lattice configurations. Ghost cells and treatment of neighbor lattices should be used to assign boundary conditions properly. Adopting multi-speed lattices culminates in larger set of solution parameters due to directional dependence of probability distribution function. Thereby, computational cost increases in simulations. The final and the most important issue for the technique is its applicability for the integrated model. As shown in Section 1.2, energy equation contains participating media radiation as a heat source. However, extra terms appear at macroscopic level in multi-speed technique, when the heat source is added into LBE. Furthermore, the conservation equations for mass and momentum also change due to these extra terms associated with the heat source. Consequently, the technique couldn't be modified to handle the source term in the correct manner.

Double population technique employs two different distribution functions for flow and thermal calculations. This increases stability of the technique and allows for independent modification of energy equation. Prandtl number and specific heat ratio can be varied with this technique. Standard lattice configurations suffice for double population technique. Therefore, it has a lower computational cost resulting in faster simulation time. Boundary treatment is straightforward and doesn't need ghost cells or neighbor lattices. Boundary conditions are usually defined with formulations based on simple bounce back method. Incorporating sub-models enables modification of energy calculations without changing those of mass and momentum. Thus, integration of the heat source is performed complying with the macroscopic equation desired for the problem. Total energy based formulation accounts for compressibility effects and viscous heating, hence eliminating one of the most important issues in double population technique. The major drawback of the technique is one way coupling of flow and thermal fields. However, there are studies having coupled models with total energy formulation [15]. As a result, the technique has the potential to be extended for fully coupled models in the future. Stability range of the model is further enhanced by the implementation of entropic formulation. This renders the model applicable also for high speed flows.

Comparing both techniques and their features, total energy based double population method is chosen as the suitable candidate for solving the flow problem with participating media radiation. It is advantageous in terms of computational time, boundary treatment, stability and simulation range. It can calculate compressibility effects and viscous heating terms as in multi-speed technique. Finally, its formulation allows for integration of the heat source without any extra or redundant terms.

The integrated model in this thesis work is based on the formulation given in Karlin et al. [8]. Flow field is decoupled from thermal calculations in the model. Prandtl number is limited to 1 as well as ratio of specific heats. Although the model is capable of handling different Prandtl number and specific heat ratios, this work adopts its simplest form. The flow under consideration is incompressible regarding the magnitude of velocities simulated in the test cases. Conveniently, formulation of the model is suitable for constant density flows [8]. However, the model may be enhanced for flows with variable density [15, 43]. Since the main concentration of this work is on the implementation of a total energy formulation with participating media, the simplest form of total energy based LBE is adopted in this thesis.

CHAPTER 4

NUMERICAL SIMULATIONS

The discrete thermal model, Eq. (41a), constructed in the previous chapter is implemented in an in-house developed code written in Matlab R2014a. This chapter includes implementation details of the model such as the algorithm and the boundary treatment. Some validation studies and comprehensive analysis of the duct flow are also included in this chapter. First, the validation of the integrated model and the developed code is performed using the well-known problem of conduction and radiation in a cavity. Then, convection and radiation case is used for validation. The results are compared with other simulations in literature. After the validation, the algorithm and the code are used to study the duct flow for various combinations of the physical parameter values. Results are presented both with and without participating media to give detailed insight into the underlying physics.

4.1 Implementation of the Model and Boundary Treatment

Implementation of the computational model is achieved in three stages that computes evolution of flow field, temperature field and participating media radiation, respectively, as shown in Figure 4.

First, the radiation model, Eq. (35), is used to calculate the evolution of radiative intensity throughout the domain with the introduction of initial and boundary conditions. Radiative intensity field is then used to obtain divergence of radiative heat transfer that appears as a source term to account for the contribution of participating media radiation in the energy equation, Eq. (41a). Calculations continue until fields reach a steady state. Radiative equilibrium is assumed at each time step during simulations.

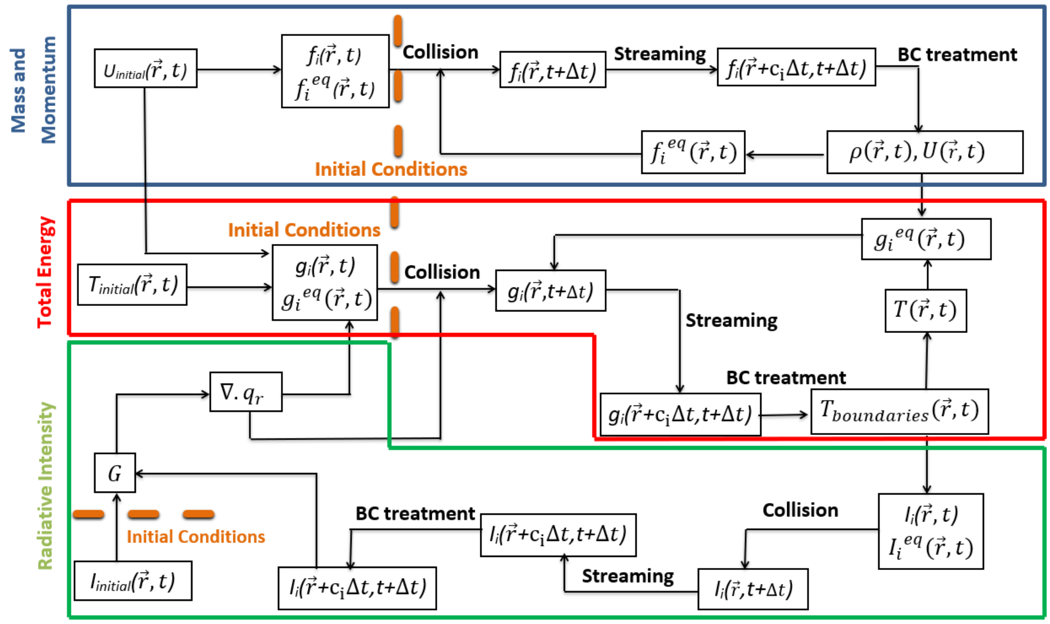

Figure 4: Model algorithm

This algorithm adopts the advantage of Asinari's model [1] that is the assumption of radiative equilibrium. Thereby, proper implementation of boundary conditions will be enough for radiative intensity to be computed in the whole computational domain. This feature brings an enormous acceleration in the computational process. The assumption of radiative equilibrium at each time step will be tested against reference cases.

a)

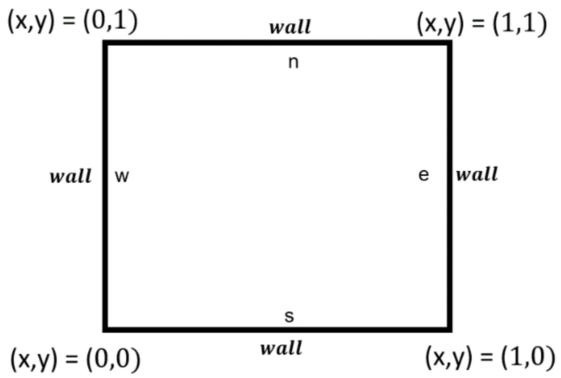

b)

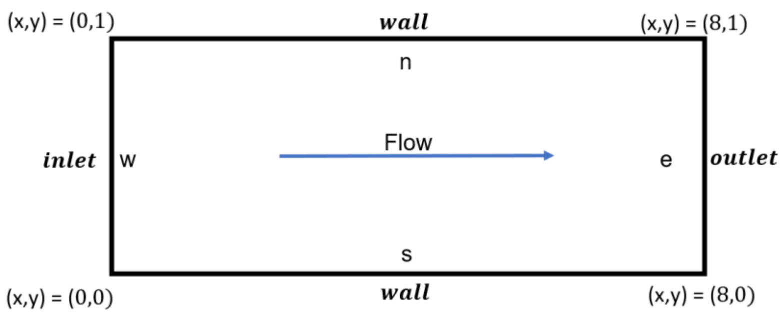

Figure 5: Computational domain and boundaries for simulations. a) Conduction – Radiation problem in a cavity. b) Convection – Radiation problem in a channel.

Initially, velocity and radiative intensity fields are set to zero, while it is set at T_{low} for the energy model, Eq. (41a). Boundary conditions are implemented according to the fundamental rules of lattice Boltzmann method. The mass-momentum model Eq. (31) uses non-equilibrium boundary conditions adopting known macroscopic values and relevant equilibrium distributions. For the energy model, anti-bounce back approach is used to define unknown population values. The radiation model, Eq. (35), adopts an approach similar to equilibrium boundary conditions [33]. All boundaries are assumed black, while the participating media is homogeneous and gray in this model. Boundary values are assigned in accordance with different flow configurations as shown in Figure 5.

Mass-momentum model uses four equations set for each boundary. All boundaries have the same form, but with different macroscopic values:

$$\rho_w = \frac{1}{1-u_w}\left[f_{1,w} + f_{3,w} + f_{5,w} + 2\left(f_{4,w} + f_{7,w} + f_{8,w}\right)\right],$$

$$f_{6,w} = \frac{1}{2}\left[\rho_w(u_w + v_w) - f_{2,w}^{eq} + f_{4,w}^{eq} - f_{3,w} + f_{5,w} + 2f_{8,w}\right],$$

$$f_{2,w} = f_{2,w}^{eq} + f_{4,w} - f_{4,w}^{eq},$$

$$f_{9,w} = \rho_w u_w - f_{2,w} - f_{6,w} + f_{7,w} + f_{4,w} + f_{8,w},$$

$$\rho_e = \frac{1}{1+u_e}\left[f_{1,e} + f_{3,e} + f_{5,e} + 2\left(f_{2,e} + f_{6,e} + f_{9,e}\right)\right],$$

$$f_{8,e} = -\frac{1}{2}\left[\rho_e(u_e + v_e) - f_{2,e}^{eq} + f_{4,e}^{eq} - f_{3,e} + f_{5,e} - 2f_{6,e}\right],$$

$$f_{4,e} = f_{4,e}^{eq} + f_{2,e} - f_{2,e}^{eq},$$

$$f_{7,e} = -\rho_e u_e + f_{2,e} + f_{6,e} + f_{9,e} - f_{4,e} - f_{8,e},$$

$$\rho_n = \frac{1}{1+v_n}\left[f_{1,n} + f_{2,n} + f_{4,n} + 2\left(f_{3,n} + f_{6,n} + f_{7,n}\right)\right],$$

$$f_{9,n} = \frac{1}{2}\left[\rho_n(u_n - v_n) - f_{2,n} + f_{4,n} + 2f_{7,n} - f_{5,n}^{eq} + f_{3,n}^{eq}\right],$$

$$f_{5,n} = f_{5,n}^{eq} + f_{3,n} - f_{3,n}^{eq},$$

$$f_{8,n} = -\rho_n v_n + f_{3,n} + f_{6,n} + f_{7,n} - f_{5,n} - f_{9,n},$$

$$\rho_s = \frac{1}{1 - v_s}\left[f_{1,s} + f_{2,s} + f_{4,s} + 2\left(f_{5,s} + f_{8,s} + f_{9,s}\right)\right],$$

$$f_{6,s} = \frac{1}{2}\left[\rho_s(u_s + v_s) - f_{2,s} + f_{4,s} + 2f_{8,s} + f_{5,s}^{eq} - f_{3,s}^{eq}\right],$$

$$f_{3,s} = f_{3,s}^{eq} + f_{5,s} - f_{5,s}^{eq},$$

$$f_{7,s} = \rho_s v_s - f_{3,s} - f_{6,s} + f_{5,s} + f_{8,s} + f_{9,s}.$$

In these expressions, the indices are based on lattice configuration D2Q9 in Figure 6 and the subscripts, e, w, n, s stand for east, west, north and south boundaries as in Figure 5, respectively.

Boundary treatment is different on the east side of the cavity and duct flow configurations. While all boundaries are solid in cavity, east side corresponds to outlet in duct flow demanding a specific approach for setting the boundary condition. In the east side boundary, axial velocity values are extrapolated from their upstream values as follows [10]:

$$u_e = \frac{4u_{e-1} - u_{e-2}}{3}. \tag{54}$$

Having three unknowns with three equations, all populations and properties associated with the mass-momentum model are defined at the outlet. Inlet doesn’t require a special treatmen, as non-equilibrium boundary condition is applicable also for inlets with a specified inlet velocity.

Thermal model utilizes anti-bounce back procedure at the boundaries. At the boundaries, there is an equation for each unknown population values in terms of the macroscopic flow quantities and reflecting known population values. Similar to mass-momentum model, it has a special treatment at the outlet. While all boundaries are treated using known macroscopic values, population values at the outlet boundary are extrapolated from upstream field values:

$$g_{2,w} = g_{2,w}^{eq} + g_{4,w}^{eq} - g_{4,w},$$

$$g_{6,w} = g_{6,w}^{eq} + g_{8,w}^{eq} - g_{8,w},$$

$$g_{9,w} = g_{9,w}^{eq} + g_{7,w}^{eq} - g_{7,w}.$$

Duct

$$g_{4,e} = \frac{4g_{4,e-1} - g_{4,e-2}}{3},$$

$$g_{7,e} = \frac{4g_{7,e-1} - g_{7,e-2}}{3},$$

$$g_{8,e} = \frac{4g_{8,e-1} - g_{8,e-2}}{3},$$

Cavity

$$g_{4,e} = g_{4,e}^{eq} + g_{2,e}^{eq} - g_{2,e},$$

$$g_{7,e} = g_{7,e}^{eq} + g_{9,e}^{eq} - g_{9,e},$$

$$g_{8,e} = g_{8,e}^{eq} + g_{6,e}^{eq} - g_{6,e},$$

$$g_{5,n} = g_{5,n}^{eq} + g_{7,n}^{eq} - g_{7,n},$$

$$g_{8,n} = g_{8,n}^{eq} + g_{6,n}^{eq} - g_{6,n},$$

$$g_{9,n} = g_{9,n}^{eq} + g_{7,n}^{eq} - g_{7,n},$$

$$g_{3,s} = g_{3,s}^{eq} + g_{5,s}^{eq} - g_{5,s},$$

$$g_{6,s} = g_{6,s}^{eq} + g_{8,s}^{eq} - g_{8,s},$$

$$g_{7,s} = g_{7,s}^{eq} + g_{9,s}^{eq} - g_{9,s}.$$

Radiative intensity values are calculated based on the radiative equilibrium assumption within the domain. The boundary treatment uses equilibrium scheme in which equilibrium distribution function is used to determine the unknown population values [33]. Adopting known macroscopic values, equilibrium distribution function is evaluated at the boundaries [40]. At the outlet boundary of the duct flow, the radiation intensity distribution function values are extrapolated from the interior lattice points.

$$I_{1,w} = I_{5,w} = I_{8,w} = I_w = 4\sigma T_w^4,$$

<u>Duct</u> <u>Cavity</u>

$$I_{3,east} = \frac{4I_{3,e-1} - I_{3,e-2}}{3},$$

$$I_{6,east} = \frac{4I_{6,e-1} - I_{6,e-2}}{3}, \qquad I_{east} = 4\sigma T_e^4,$$

$$I_{7,east} = \frac{4I_{7,e-1} - I_{7,e-2}}{3}$$

$$I_{2,s} = I_{5,s} = I_{6,s} = I_s = 4\sigma T_s^4,$$

$$I_{4,n} = I_{7,n} = I_{8,n} = I_n = 4\sigma T_n^4.$$

4.2 Conduction with Participating Media in a 2D Cavity

Conduction in a 2D cavity with participating media radiation is a widely studied problem in literature. This problem involves a computational domain with one hot surface at the lower wall and three cold surfaces. Temperature distribution between hot and cold boundaries can be constructed in closed form for the pure conduction case. This profile is also calculated with the model and it is be used to assess the effects of the participating media radiation by varying the parameters such as extinction coefficient, optical thickness, absorption and scattering coefficients.

Figure 4a shows the computational domain for the 2D cavity problem. South boundary is hot with temperature of $2T_{low}$, and other boundaries are cold and have temperature value of T_{low}. Physics associated with the participating media radiation depends on the radiation parameters, thermo-physical properties of the material and the boundary temperature values. A dimensionless number, *N*, Planck number is used to account for the overall effects of these parameters on physics in this problem:

$$N = \frac{k\beta_{ext}}{4\sigma T^3}. \quad (55)$$

Mishra et al. [21] conducted a comprehensive study for conduction – participating media radiation in 2D cavity problem. Their results are based on a lattice Boltzmann solver and adopted as a reference study in this section. The simulations and the comparisons are performed for various values of Planck number N, extinction coefficient β_{ext} and single scattering albedo , φ.

First, the computational model is tested for grid dependency in the case of $\beta_{ext} = 1$ and $N = 0.01$. The iterations are continued until variation between successive iterations is less than 1e-10. Grid dependency analysis is performed based on the temperature distribution at the vertical midline of the domain, (T_c) and its 2-Norm normalized with respect to reference solution.

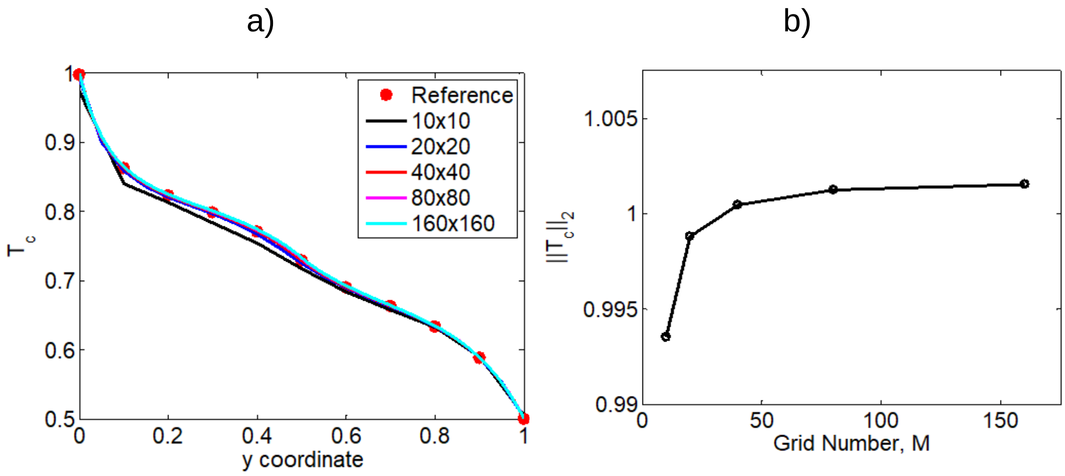

Figure 7: Grid dependency. a) Temperature Distribution. b) 2-Norm of Centerline Temperature.

As shown in Figure 7, the convergence to a grid independent solution is achieved. Figure 7a demonstrates temperature variation with respect to different grid sizes. While there is substantial variation of results with 10 and 20 grids, temperature distribution doesn't change with spatial resolutions higher than 40 grids. The trend also reflects Figure 7b in which 2-Norm of temperature distribution is shown. Results show substantial variation with spatial resolutions lower than 40 grids. While there is a small variation for the resolution between 40 and 100 grids, increasing the grid resolution beyond 100 doesn't create any appreciable effect on the solution. Considering the computational efficiency and the small variation in results, 40x40 grid structure is employed in the subsequent analyses.

Computational time for 40x40 grid is 47.54 seconds using a personal computer having 2.30 GHz multi-processor with 8 cores. The code structure is optimized in order to exploit the maximum performance in Matlab through vectorization and matrix computations with minimum use of loops. Computational performance of the code can be increased further through lower-level programming languages as C++ or C#. However, the focus of the study is on the modification of the total energy model for duct flow with participating media radiation. Therefore, Matlab code is used for the entire study without spending additional time for coding.

Figure 8 demonstrates model results along with the reference solution [21]. Ref. [21], adopts different methods to solve the problem. These methods are called as FVM-FVM and LBM – FVM. In the first method, both energy and radiation is calculated with FVM. LBM – FVM method employs LBM for energy calculation, whereas it uses FVM for radiation. All of these methods are included in Figure 8 to provide a better insight for solution accuracy of the model developed in the thesis. As shown in Figure 8, the simulation results are comparable to reference cases [21].

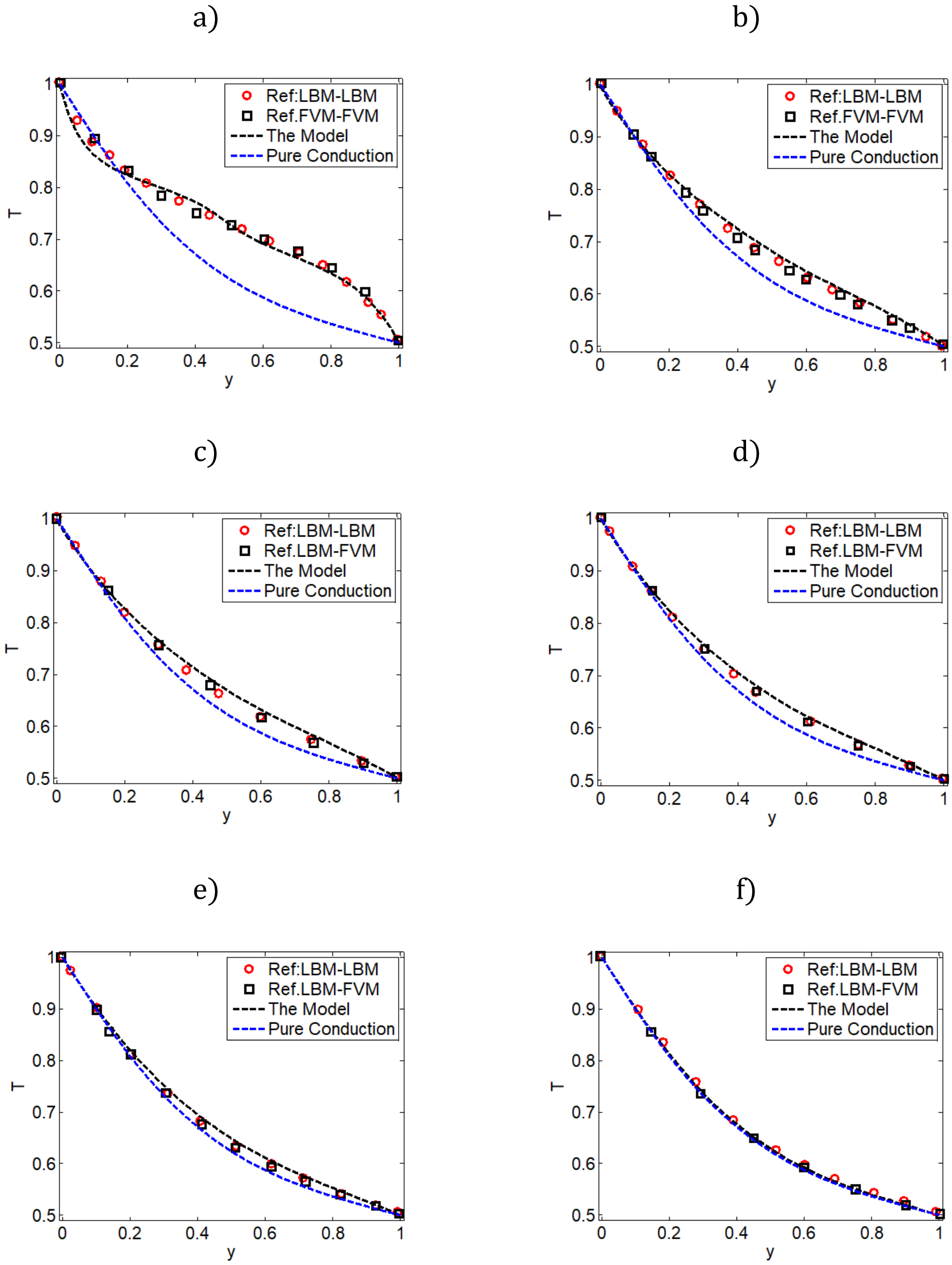

Figure 8: Simulation cases for conduction radiation problem in a cavity.

a) N=0.01, $\beta_{ext} = 1, \varphi = 0$; b) N=0.1, $\beta_{ext} = 1, \varphi = 0$; c) N=0.1, $\beta_{ext} = 1, \varphi = 0.3$; d) N=0.1, $\beta_{ext} = 1, \varphi = 0.5$; e) N=0.1, $\beta_{ext} = 1, \varphi = 0.7$; f) N=0.1, $\beta_{ext} = 0.1, \varphi = 0$.

Temperature profile along the vertical midline exhibits steeper changes, when Planck number, N, is lower. Higher Planck number ends up with smoother temperature distribution similar to pure conduction case.

Single scattering albedo controls the amount of radiation being absorbed and scattered. It is clear that as single scattering albedo increases, temperature profile becomes closer to the pure conduction case. Absorption is the main factor facilitating temperature rise due to participating media radiation. Higher single scattering albedo causes loss of more radiation energy due to scattering. Thereby, effect of participating media radiation becomes less prominent for higher single scattering albedo values.

Extinction coefficient is related to optical thickness of the medium. As its value is lower, the medium becomes optically thinner. Effect of the radiation decreases in an optically thin medium. Therefore, very low extinction coefficient values, such as 0.1, cause a temperature profile being similar to that of pure conduction case, Figure 8f.

A numerical comparison is also performed based on the percent maximum error with respect to the reference [21] in Table 6. As shown in the table, maximum error is less than 3% in all cases compared to LBM-LBM solutions of the reference. The variation is similar with respect to different modeling techniques regarding small variation in reference solutions.

Table 6: Percent maximum error for conduction – radiation case

Case	a	b	c	d	e	f
% Maximum Error	1.5%	2.6%	1.7%	1.3%	0.9%	0.8%

4.3 Convection with Participating Media in a Duct

The second step for validation includes cases with convection and radiation. Four cases are defined for validation from Ref. [28]. Computational domain is a duct with a length to height ratio of 10. Top and bottom walls are hot, whereas there is a relatively cold flow between inlet and outlet. Temperature values are T_0 for cold boundaries, while it is $3T_0$ for hot boundaries. Similar to cavity case, radiation parameters are expected to have an impact on the solution. Simulations are performed for Reynolds number (Re) of 71 as defined below

$$Re = \frac{U_0 M}{v} \tag{56}$$

and Prandtl number of 1. Extinction coefficient is 1, as single scattering albedo changes from 0 to 0.65. Planck number is set to 0.01. Following Figure 9, 40x400 lattices are employed in grid structure. Grid structure is limited with solution stability in its minimum value. Therefore, 20x200 lattices are used as the coarsest grid structure in grid dependency analysis. There is substantial difference between 20x200 lattices and 40x400 lattices. Further increase of lattices doesn't cause a change in temperature profile. As a result, 40x400 lattices are adopted as grid structure in this problem. Temperature at hot boundaries is $3T_0$, whereas fluid enters the domain with a temperature of T_0. Outlet is represented as outflow in which flow properties are extrapolated from upstream. Convergence criteria are the same as that of the cavity case. Both flow field and radiative transfer calculations are iterated, until change in solutions becomes less than 1e-10 between successive iterations. Computational time required for each case is around 832 seconds with the same computing resource mentioned in previous section.

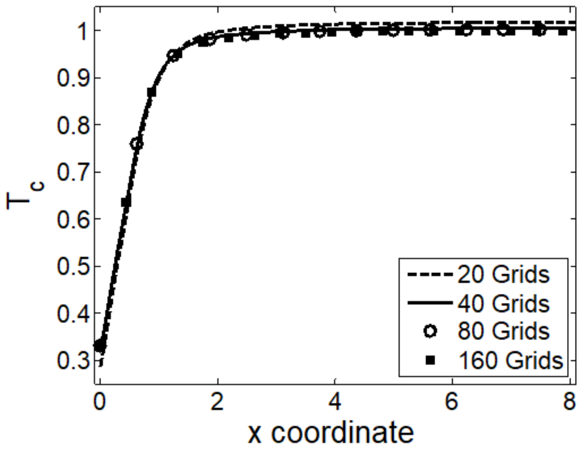

Figure 9: Grid dependency for the reference problem with convection and radiation.

Cases are also solved through a commercial CFD code to better interpret solution accuracy of the model developed in the thesis. Fluent v19 is used in this study. Pressure based solver is adopted for the problem. Radiation is modeled through DOM approach. Boundary values are defined accordingly so that simulation ends up with same Re number and Planck number as in the reference problem. 50x500 elements are used as the grid structure. Blackbody temperature is also defined for inlet and outlet boundary conditions regarding reference temperature is the maximum temperature in LBM solutions. Detailed information about the macroscopic properties in the solution domain will be provided in Section 0.

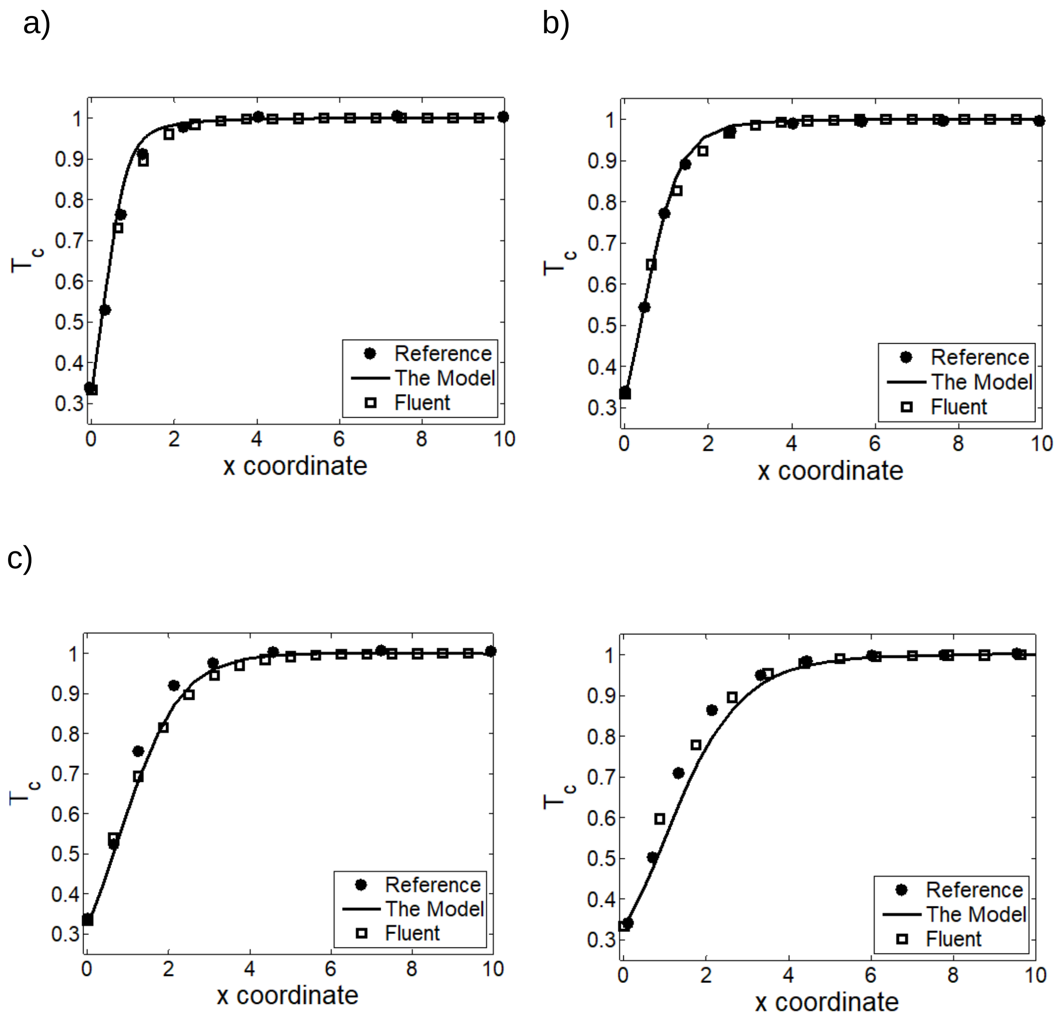

Figure 10: The temperature profiles along the horizontal midline for the current simulations (LBM) in comparison to Ref. [14] for convection-radiation problem in a duct. a) $\varphi = 0$; b) $\varphi = 0.35$; c) $\varphi = 0.65$; d) $\beta = 0.5$.

Temperature distribution through the horizontal midline is the parameter for investigation. As seen in Figure 10, reference solution and the model show a good agreement in terms of solution trend and numerical values. Fluent results are also similar to both solutions in all cases. The percent maximum error in temperature is lower than 8% with respect to reference solution for the given temperature range, Table 7.

Table 7: Percent maximum error for convection – radiation case

Case	$\varphi = 0$	$\varphi = 0.35$	$\varphi = 0.65$	$\beta^* = 0.5$
% Maximum Error	4.7%	2.5%	6.9%	7.6%

4.4 Interpretation of Results in terms of Macroscopic Properties

Lattice Boltzmann Method solves all problems in mesoscopic scale. This corresponds to macroscopic solutions in lattice units. Therefore, unit conversion is also necessary for simulations.

LBM problems are specified according to non-dimensional numbers. In a duct flow with participating media, three non-dimensional numbers are defining for the overall solution. These are Re number, Pr number and Planck number.

In order to have a better explanation, one shall first consider duct flow without participating media radiation. Non-dimensional parameters are Re number and Planck number. Simulation domain is the same as solved in Section 4.3, but with macroscopic values. This corresponds to wall temperatures of 900 K, and inlet temperature of 300 K. Duct height is 1 m, while its length is 10 m. Material properties of fluid is defined as 1.65 W/mK for thermal conductivity, 1000 j/kgK for specific heat under constant pressure and 1.0 kg/m^3 for density. Kinematic viscosity is 0.00165 m^2/s. Based on the geometry and viscosity, inlet velocity is assigned as 0.11715 m/s.

a) b)

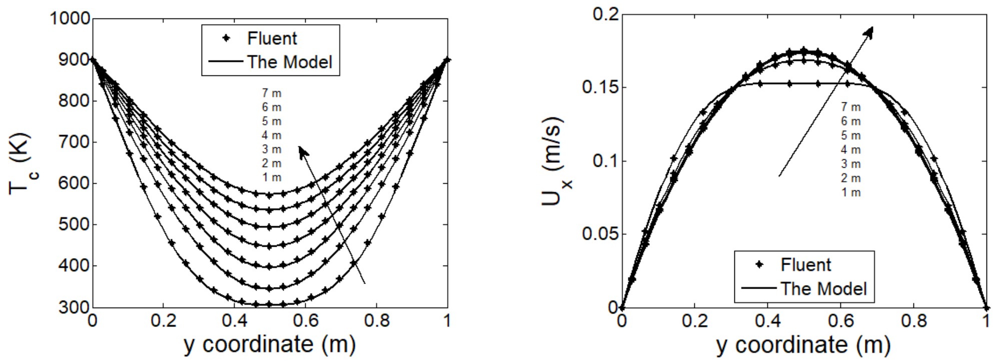

Figure 11: Duct flow without participating media in macroscopic units. a) temperature profile, b) velocity profile through the duct at $x = 1 - 7$ m. axial distances.

As seen in Figure 11, the model and Fluent solutions match each other. Velocity profiles and temperature distribution throughout the domain is almost the same for both solutions. It is clear that LBM solves for a non-dimensional problem. If non-dimensional numbers are the same, it approaches the macroscopic solution.

If participating media is present, Planck number becomes an additional parameter that shall be defined in the domain. Using an extinction coefficient of 1, Planck number is 0.01 for this set up. Same Re numer and Pr number is preserved as in the previous case ($Re = 71$, $Pr = 1$). Single scattering albedo is 0, whereas absorption coefficient is 1.

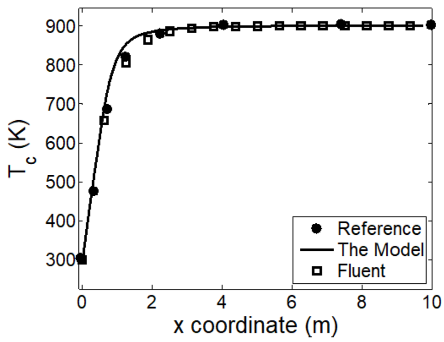

Figure 12: Duct flow with participating media in macroscopic units.

Figure 12 represents results demonstrated in Section 4.3 but with macroscopic values. As seen in graph, once non-dimensional parameters are considered, LBM again converges to macroscopic solution. Other words, lattice Boltzmann method requires correct set up of non-dimensional parameters to match a physical problem at macroscopic scale. If non-dimensional numbers are the same for a problem, LBM and macroscopic models solve the same problem [33].

4.5 Duct Flow with Participating Media

4.5.1 Problem Definition

Having presented the implementation details of the computational model and performed validation in comparison to the available cases in literature, convection with participating medium radiation in duct flow problem will be studied in more details by varying physical parameters in this section. Figure 13 shows the computational domain and the boundaries of the duct geometry with a chosen aspect ratio of 8. Walls have higher temperature than the fluid and participating media radiation is present in the domain with absorption, scattering and emission. Gravity is neglected regarding the forced flow through the channel.

In order to investigate the effect of participating media radiation in duct flow, numerical simulations are performed over a wide range of parameter set, namely, Reynolds number, extinction coefficient and single scattering albedo, to determine their effects and contributions. Reynolds number is calculated based on Eq. (56). Since the kinematic viscosity and thermal diffusivity are each assigned a value of 0.04 in all cases, the uniform inlet flow velocity or grid number M is adjusted for the specified value of the Reynolds number.

The values are assigned to the simulation parameters so that Planck number is 0.01 for the case in which extinction coefficient equals to 1. Since the thermal conductivity is fixed for all cases, Planck number changes with the extinction coefficient.

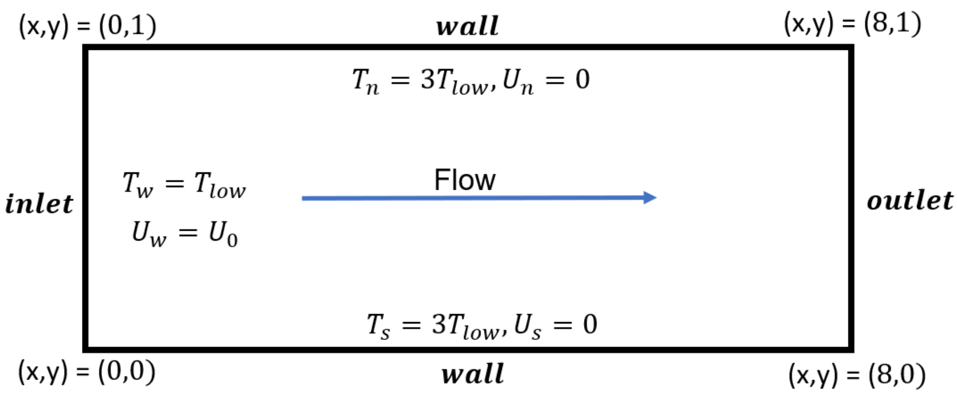

Figure 13: Computational domain for duct flow

First, the grid dependency is tested based on the temperature distribution T_c along the horizontal midline of the duct and grid number M along the height of the domain, because the interaction between the flow field and the duct walls mainly occurs along the vertical y-direction. Analyses are conducted with Re number of 100. Having the same kinematic viscosity for all cases, inlet velocity is adjusted as the grid number is varied to fix Re at 100. Table 8 lists the uniform inlet velocity values and the corresponding grid numbers.

Table 8: Inlet velocity for different grid numbers

Grid Number, M	U_0
25	0.16
50	0.08
100	0.04
200	0.02

Figure 14 shows the convergence of temperature distribution through the horizontal midline in 2-norm as grid number increases. As shown in the figure, 2-norm of centerline temperature exhibits a considerable change between the cases with $M = 25$ and 50. The variation becomes smaller with $M = 50$ and 100, and results are almost the same for cases of $M = 100$ and 200. Further increase in the grid number does not have considerable effect on the solution. Considering computational efficiency and accuracy, $M = 100$ is selected as default grid structure for the problem.

$$Error = \frac{\left\|T_{c,new} - T_{c,old}\right\|_2}{\left\|T_{c,old}\right\|_2} \tag{57}$$

Figure 14b shows rate of convergence for the problem. The integrated model exhibits a rate of convergence being slightly higher than 2nd order with respect to relative error in $||T_C||_2$ as indicated in Eq. (57).

a) b)

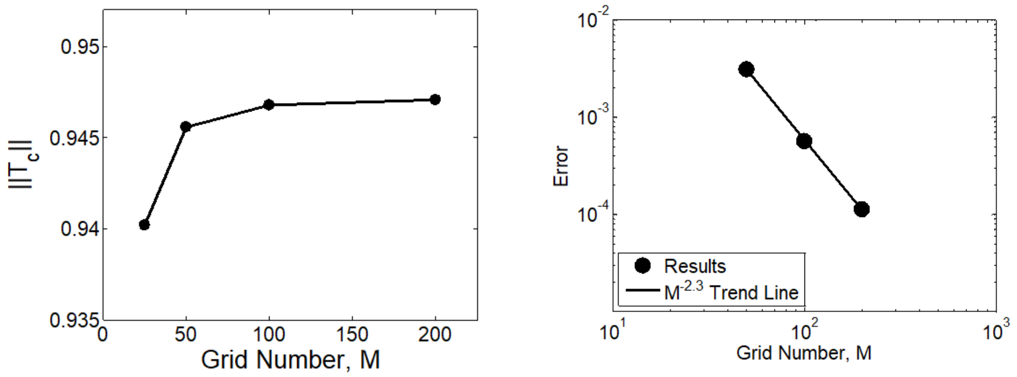

Figure 14: Grid dependency for duct flow. a) 2-Norm of temperature distribution through the horizontal midline, $||T_C||_2$.b) Rate of convergence with respect to relative error.

Interpretation of results for varying Re number as defined in Eq. (56) requires evaluation of the effect of grid resolution on the inlet velocity. Inlet velocity is a defining parameter for adjusting velocity magnitude in the solution. It is known that LBM is sensitive to velocity magnitude in the domain [33]. In order to attain a grid independent and an accurate solution, inlet velocity should be around 0.04 for the problem investigated in this paper (see Table 8). Therefore, grid number is adjusted to have velocity magnitude of 0.04 at the inlet for all cases.

4.5.2 Effect of Re Number

Re number indicates the relative dominance of inertial forces over viscous forces. Thereby, it plays an important role in interpreting the effect of the convection. Participating media radiation is analyzed with different Re numbers to have an insight about its contribution under different Re numbers. Three different Re number values, namely 100, 200 and 400, are adopted for this analysis. While keeping all other parameter values fixed, grid number M is increased to achieve these Re values.

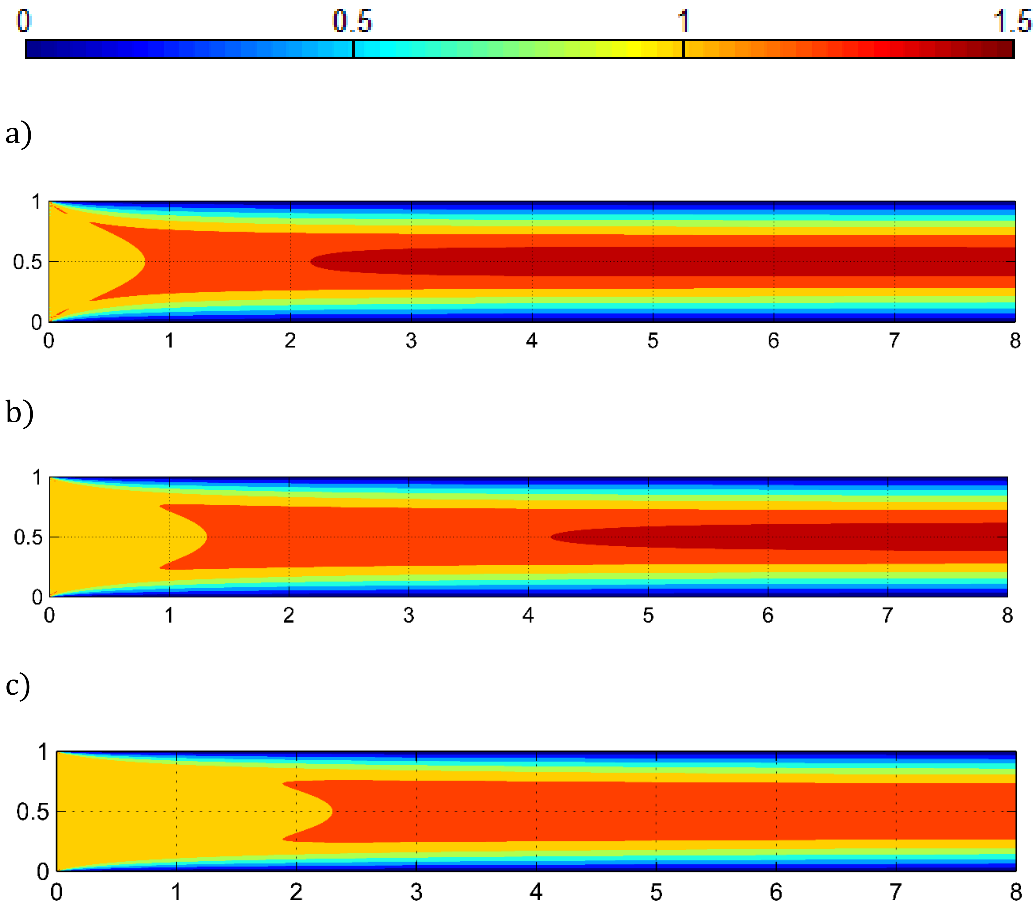

Figure 15: Velocity contours for different Re numbers for U/U_0 .

a) Re 100. b) Re 200. c) Re 400.

The resulting velocity distributions are shown in Figure 15. As expected, the entrance region is longer at higher Re values. Velocity gradient in x - direction is higher in entrance region, while it decreases through the domain, as shown in Figure 16. The flow field becomes fully developed in case of $Re = 100$, while it is developing for $Re = 200$ and $Re = 400$ within the duct length.

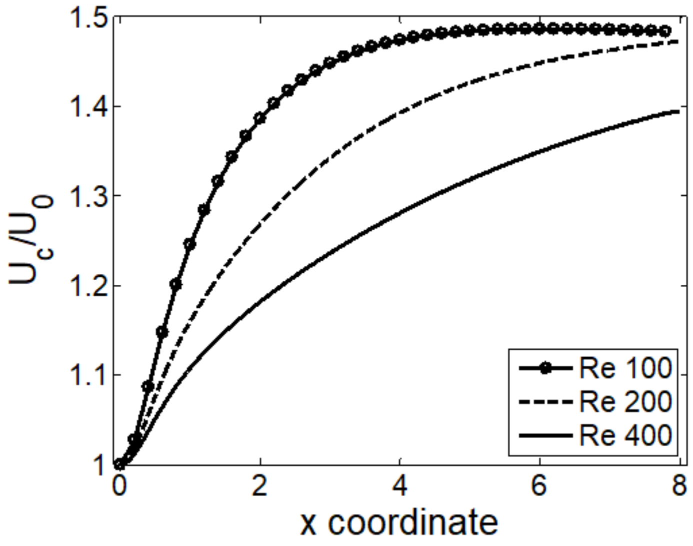

Figure 16: Velocity distribution through the duct for different Re numbers.

This is consistent with the estimate of the entrance length l_e given in [26],

$$\frac{l_e}{H} = 0.06Re. \tag{58}$$

Regarding Eq. (58), the fully developed region begins at around $x = 6$ for $Re = 100$. As estimated by Eq. (58), and as shown in Figure 11, it takes longer duct length to achieve fully developed velocity distribution for $Re = 200$ and $Re = 400$.

Figure 17 - Figure 18 show temperature contours throughout the whole domain for duct flow both with and without participating media radiation for Re number values, 100, 200 and 400, respectively. Participating media radiation has a notable impact on temperature distribution, as temperature rises suddenly with the presence of participating media radiation enhancing heat transfer from hot walls. This causes increasing uniformity in temperature closer to the entrance region. Effect of Re number is prominent both with and without participating media radiation. For pure

convection cases, the transfer of heat from hot walls is slower and their effect is felt closer to the walls, more so as Re increases. The main difference is observed in the entrance region among the three cases, when participating media radiation is present. For higher Re number, the entrance region is longer and covers almost half the duct length for $Re = 400$.

a) Re 100

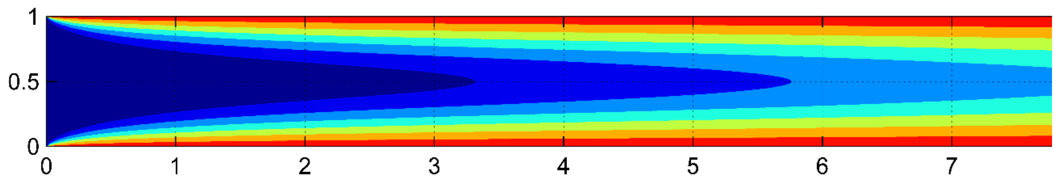

b) Re 100

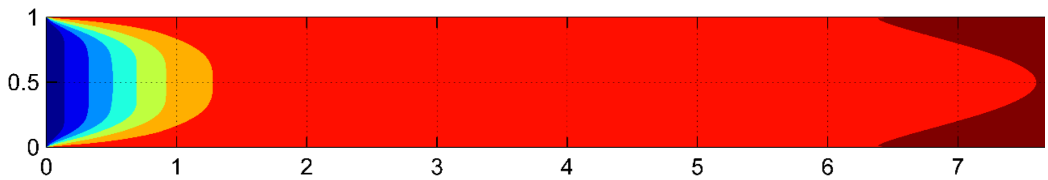

Figure 17: Temperature contours in the duct. a) Pure convection. b) Convection and Radiation.

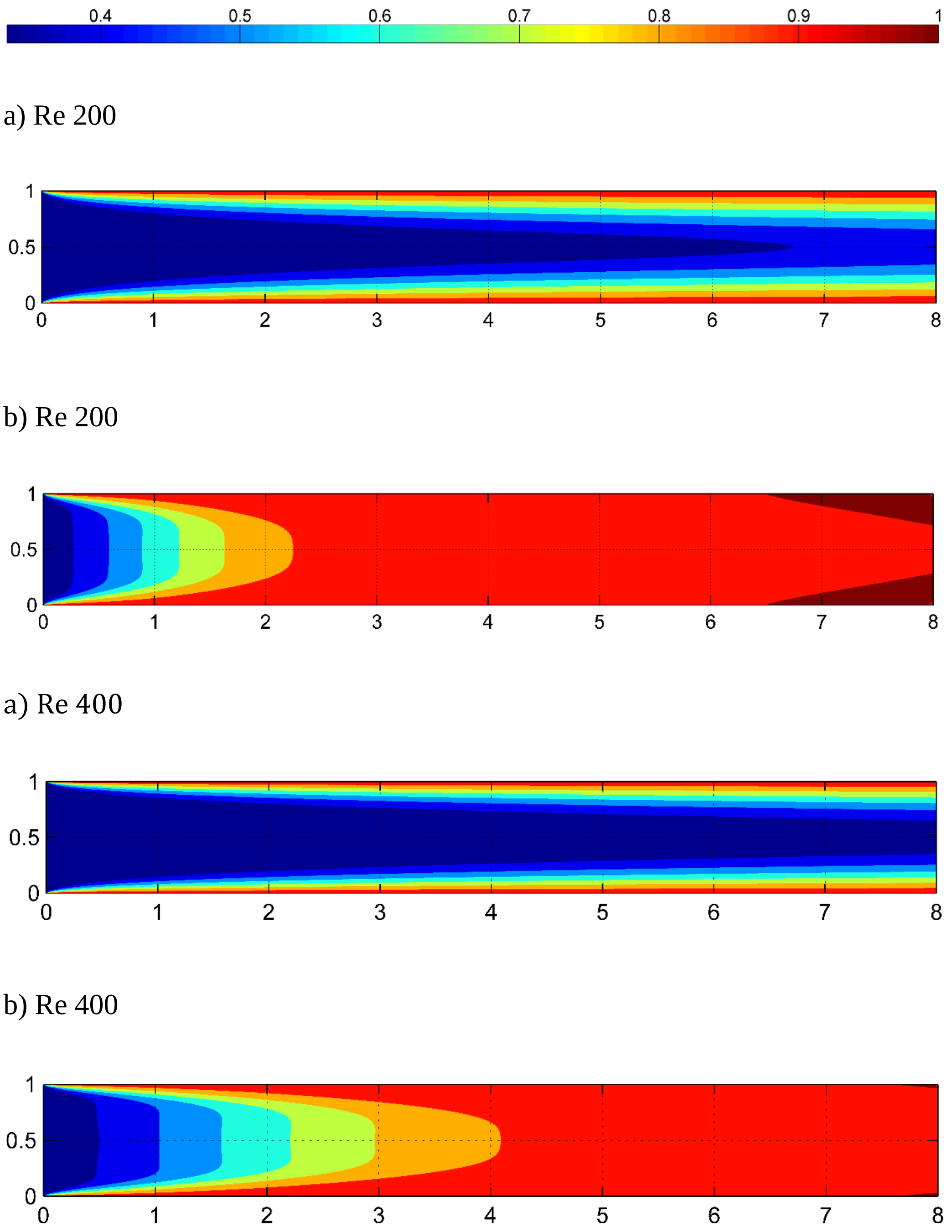

Figure 18: Temperature contours in the duct. a) Pure convection. b) Convection and radiation.

Distance required for thermal equilibrium is also affected by Re number. Thermal equilibrium region shifts towards the outlet, as Re number increases.

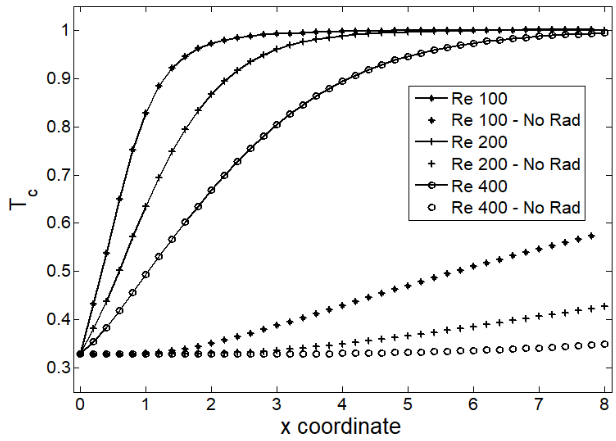

Figure 19: Temperature distribution at the horizontal midline.

Figure 19 shows temperature values along the horizontal midline of the domain with and without participating media radiation. As it is shown, temperature profiles have a steep increase at the outset with the presence of the participating media radiation. Pure convection cases end up with substantially lower temperature values throughout the duct.

Thermal boundary layer development is the main mechanism for hot walls to affect flow temperature in pure convection. The estimates of the thermal entry length $l_{e,th}$ given in [27] by

$$\frac{l_{e,th}}{H} = 0.05RePr, \tag{59}$$

is around $x = 5, 10, 20$ for $\mathrm{Re} = 100, 200, 400$ in pure convection case. This is consistent with current simulations based on the solution trend of Nu number, Figure 20. Nu number is calculated using Eq. (60) and Eq. (61) [44].

$$Nu = \frac{hH}{k} \tag{60}$$

where h is convection coefficient, k is thermal conductivitiy and H is the channel height. Determining the convection coefficient h requires Eq. (61):

$$h(T_{wall} - T_{mean}) = k \frac{\partial T}{\partial y}\bigg|_{wall} \approx k \frac{\Delta T}{\Delta y}\bigg|_{wall}, \qquad T_{mean} = \frac{\sum_{i=1}^{M} T_i U_{x,i}}{\sum_{i=1}^{M} U_{x,i}} \qquad (61)$$

Eq. (60) calculates Nu number based on the wall temperature in the domain, temperature gradient near wall and mean temperature of the flow [44]. Mean temperature of the flow is defined with respect to flow temperature and flow velocity in the x direction. Also having convection coefficient, h, via Eq. (61) Nu number is computed using Eq. (60). Figure 20 shows the variation of Nusselt number (Nu) along the duct in the pure convection case. Nu number is expected to approach to the value of 3.66 in the fully developed region [45]. As it is shown, the flow becomes thermally fully developed around $x = 5$ for Re 100. However, a longer duct is necessary to have a developed thermal boundary layer for cases with Re $=$ 200 and 400.

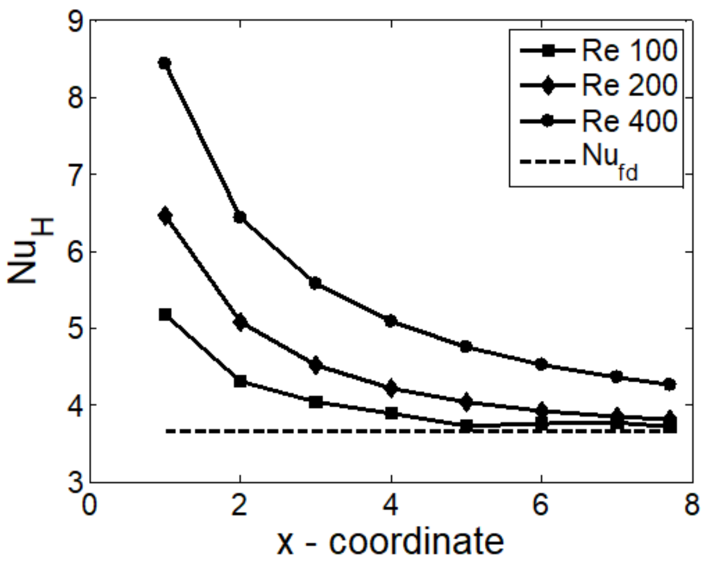

Figure 20: Nusselt number through the duct.

Participating media radiation introduces an additional mechanism for heat transfer through photons that is faster than thermal boundary layer development in pure convection cases. Thus, centerline temperature suddenly rises in the presence of participating media radiation. Even at $\mathrm{Re} = 400$, there is a clear impact of hot walls on fluid temperature with participating media radiation.

4.5.3 Effect of Single Scattering Albedo (φ)

Radiative energy can be absorbed, emitted and scattered in participating media radiation. Single scattering albedo characterizes the scattering and absorption of the participating media radiation. In order to assess the effect of the single scattering albedo on the overall heat transfer, five different values of single scattering albedo, namely, $\varphi = 0.0,\ 0.25,\ 0.5,\ 0.75,\ 1.0$, are used in this section. In the case of $\varphi = 0.0$, all radiative energy is absorbed without any loss. On the contrary, the case of $\varphi = 1.0$ corresponds to a total loss of radiative energy to scattering, hence there is no contribution of participating media radiation on heat flow.

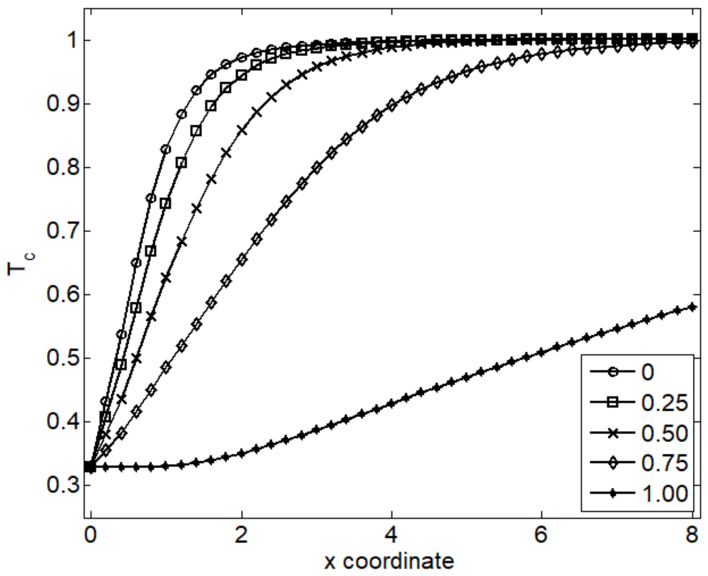

Figure 21: Temperature distribution at the horizontal midline with different single scattering albedos, $\varphi = 0, 0.25, 0.50, 0.75, 1.00$.

As shown in Figure 21 the temperature values along the horizontal midline of the duct decrease with higher single scattering albedo values. Aligned with the mathematical structure of the energy equation, higher single scattering albedo reduces contribution of participating media radiation due to lower absorption. As a result, temperature rise is slower throughout the duct. Temperature distribution also becomes equal to that of pure convection for $\varphi = 1.0$.

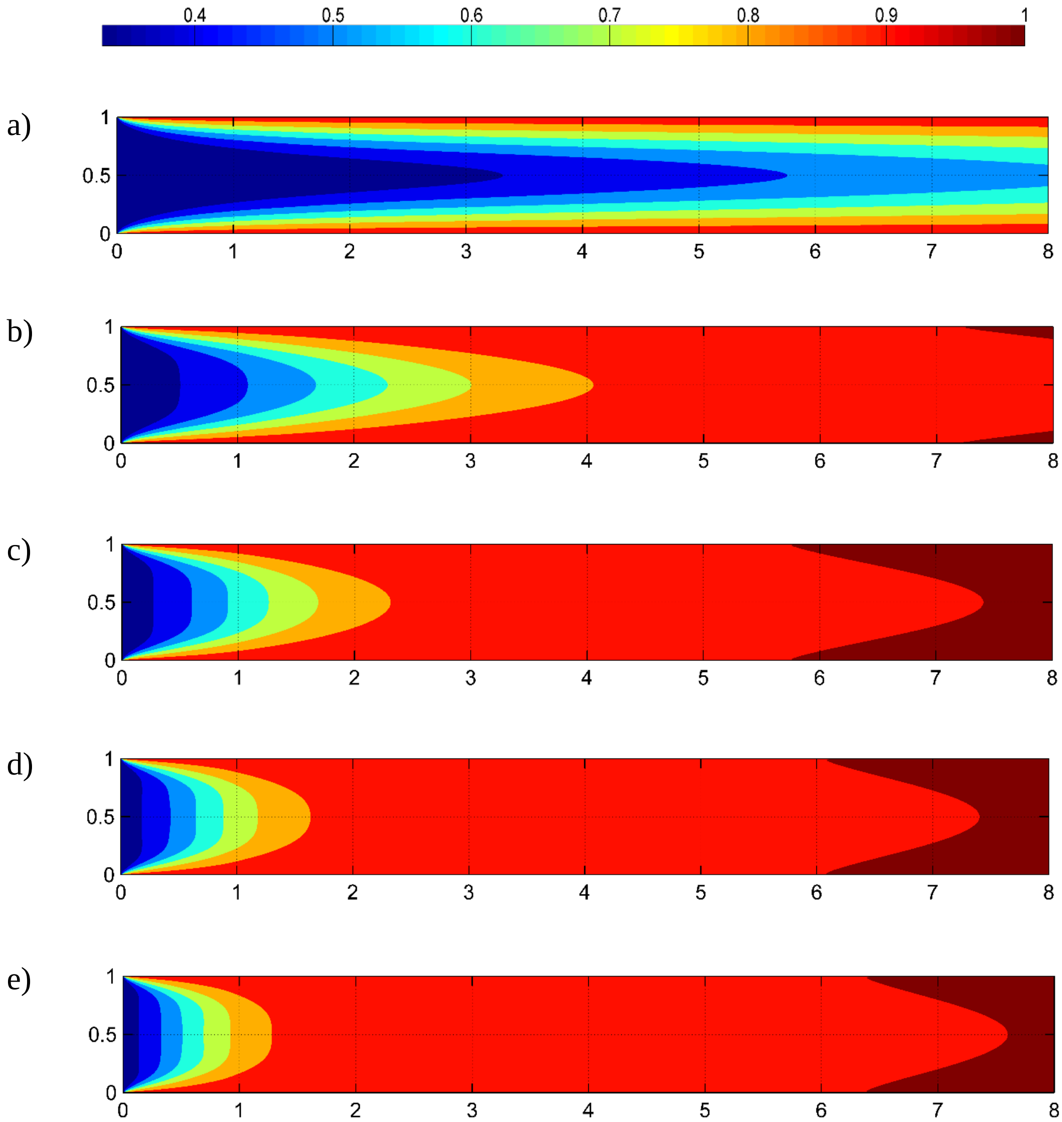

Figure 22: Temperature contours at different single scattering albedos.

a) $\varphi = 1$. b) $\varphi = 0.75$. c) $\varphi = 0.5$. d) $\varphi = 0.25$. e) $\varphi = 0$.

The temperature contours in Figure 22 are reflecting the tendency in the horizontal midline, namely, temperature increase is slower for higher single scattering albedo values. As radiation energy is scattered with increasing single scattering albedo, effect of the participating media radiation decreases. It is worth noting that even small amount of absorption causes drastic change in the temperature distribution throughout the domain compared to the pure convection case ($\varphi = 1$).

4.5.4 Effect of Extinction Coefficient ($\boldsymbol{\beta_{ext}}$)

Participating media radiation depends on the attenuation throughout the domain. Total attenuation is characterized by the extinction coefficient. It includes absorption and scattering of radiation energy. Six different extinction coefficient values are selected in this section, namely, $\beta_{ext} = 1.0,\ 2.5,\ 5.0,\ 10,\ 20.,\ 30$. These values of extinction coefficient are selected so that the analyses cover a wide range from optically thin to optically thick media, where optical thickness changes proportionally with the extinction coefficient. Absorption is the main mechanism in attenuation, coupling thermal calculations and radiative energy propagation [29]. Therefore, single scattering albedo is taken as 0 for all cases to ascertain overall impact of participating media radiation depending only on the extinction coefficient without any loss during propagation of radiation energy.

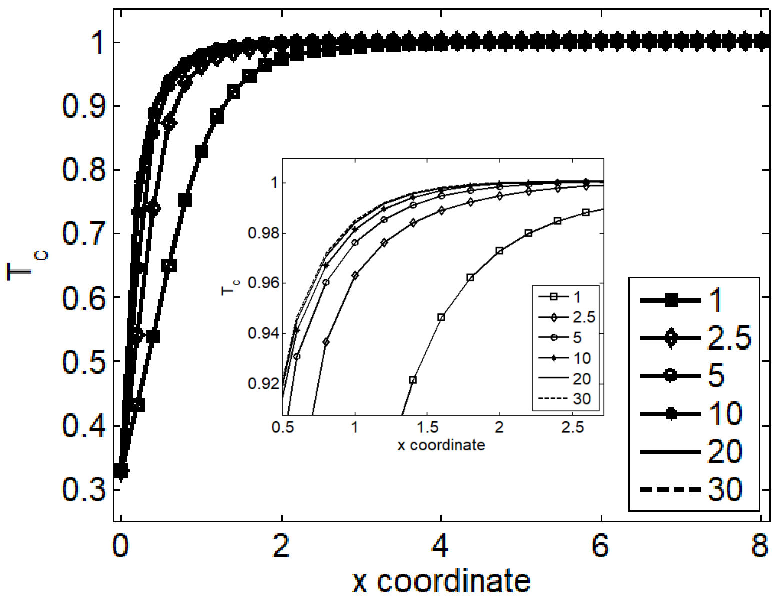

Figure 23: Temperature distribution at the horizontal midline for different extinction coefficient values, $\beta_{ext} = 1, 2.5, 5, 10, 20, 30$. The inset focuses on a smaller region for clarity.

Figure 23 shows temperature distribution along the horizontal midline in the duct. It is clear that effect of the participating media radiation is more prominent, when extinction coefficient is higher. Temperature distribution demonstrates abrupt changes in the proximity of inlet at higher extinction coefficient values. As the value of the extinction coefficient is further increased, no more visible change is observed in the temperature distribution.

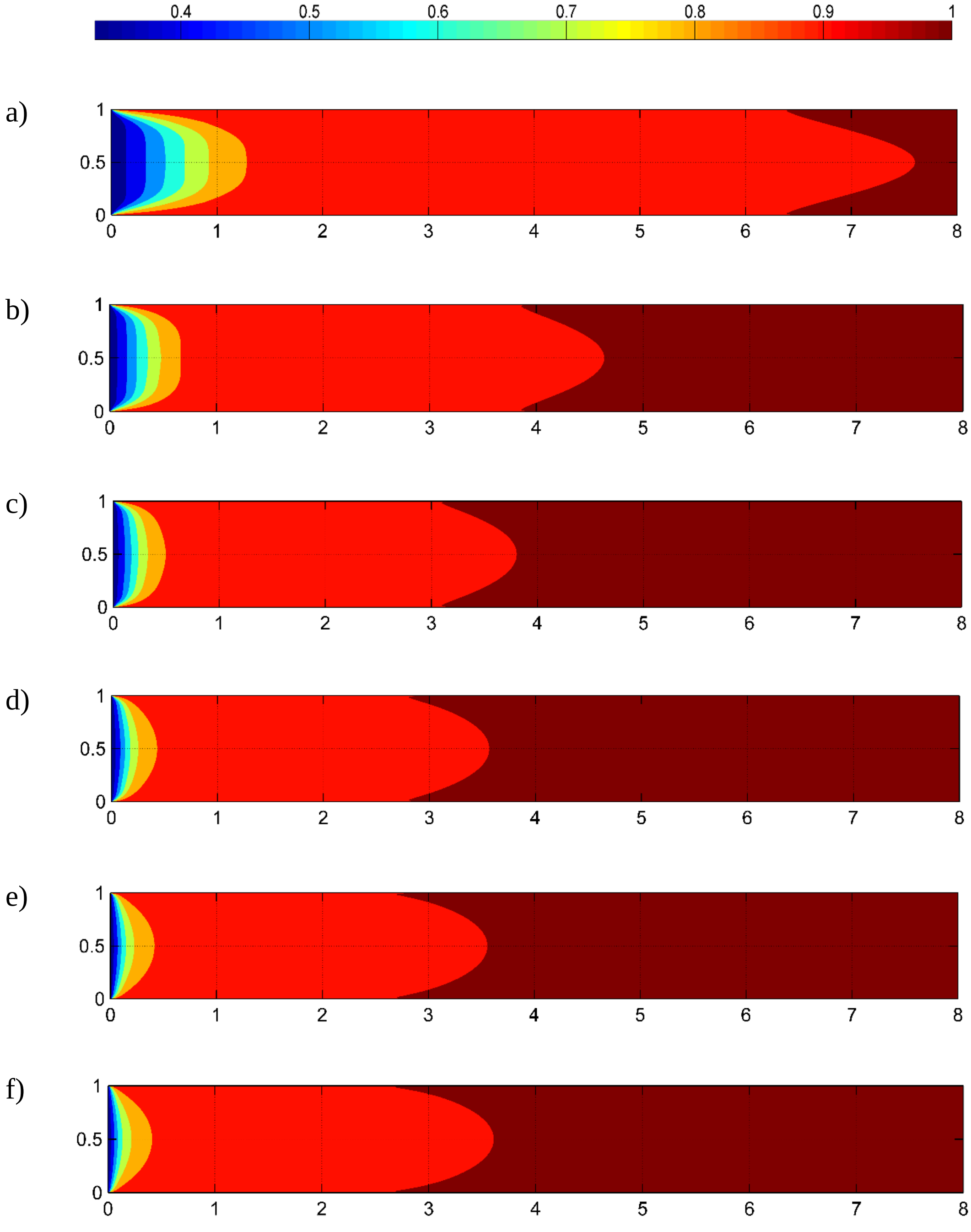

Figure 24: Temperature contours at different optical thickness values.

a) $\beta_{ext} = 1$. b) $\beta_{ext} = 2.5$. c) $\beta_{ext} = 5$. d) $\beta_{ext} = 10$. e) $\beta_{ext} = 20$. f) $\beta_{ext} = 30$.

Temperature contours in Figure 24 show the effect of extinction coefficient in the whole domain. In all cases, flow reaches thermal equilibrium within the length of the duct. However, the initial cases result in a significant reduction in distance to reach thermal equilibrium. Variation between the cases diminishes with extinction coefficient values higher than 5 except for the region in the proximity of the inlet. As β_{ext} is higher than 5, participating media radiation enters diffusive regime. In diffusive regime, the effect of participating media radiation is more pronounced in comparison to pure convection.

CHAPTER 5

CONCLUSIONS

Total energy based double population LBM is implemented in heat flow problems with participating media radiation. Participating media radiation arises due to high temperature fluid flow. These cases mostly contain all modes of heat transfer. Therefore, an integrated model is necessary for numerically simulating multi-mode heat transfer phenomena.

Accommodating all advantages of total energy formulation, this work extends its usage to participating media radiation problems. A proper formulation is provided, and an algorithm is developed for the discrete model. After the validation of the formulation and the computational model is performed using the available reference cases in literature, duct flow with hot walls is investigated in details regarding the effects of different control parameters on participating media radiation. The simulation results are consistent with the physics expected in each case, and they provide an essential insight to the duct flow problem with participating media radiation. The simulations ascertain effect of Re number on the heat flow structure that higher Re number values cause longer path to thermal equilibrium. The temperature profile throughout the duct becomes smoother, as Re number increases. Single scattering albedo is important due to its indicating the ratio of scattering and absorption in total attenuation. Absorption is one of the main factors for the contribution of radiation energy propagation in total energy. Consequently, contribution of participating media radiation is lower for higher single scattering albedo values. The presence of participating media radiation, however, is noticeable on the temperature distribution in the domain even with high values of single scattering albedo. Extinction coefficient represents total attenuation in the domain and can also be interpreted as optical thickness of the medium. Some cases are analyzed to reveal the change in temperature distribution in the domain with respect to different extinction coefficients and optical thicknesses. It is clear that participating media radiation is more pronounced, as the media is optically thicker, and attenuation is higher.

The results presented are promising for the model proposed in this thesis study. However, future extensions are still necessary and valuable for industrial applications. For example, the model can be adopted for variable Prandtl number and polyatomic gases. There are some extensions of the model for compressible flow calculations with fully coupled flow field and thermal calculations as in [15]. These extensions are useful in particular for high-speed compressible flows. Therefore, future studies shall concentrate on fully coupled LBM solution for flow problems with participating media. Parallel processing has a remarkable potential for modeling problems involving complicated physics. The computational model for heat flow problems with participating media radiation benefits from parallelization in real life applications as well. Consequently, it is considered as another area of study for improving the model in the future. 3D models are necessary for more realistic heat flow problems with participating media radiation. Thereby, the model can be enhanced to account for 3D geometries. Participating media radiation and its modeling using lattice Boltzmann method is an active research area. By following the progress in this area in literature, more robust and detailed participating media formulations can be integrated into the model.

Irregular geometries are also of interest for more realistic numerical simulations. LBE involving specific characteristic velocity directions facilitates the implementation of Finite Volume or higher order Discontinuous Galerkin methods. With the success of the computational model presented in this thesis, these more flexible and higher order numerical methods may be used to increase the versatility of the method.

The increased numerical stability of LBM by taking H-theorem into account in the discretization process of the equilibrium population distribution as implemented in this thesis can further be enhanced by utilizing the dynamic relaxation feature of the entropic approach in an extension of this study [15].

REFERENCES

[1] P. Asinari, S. C. Mishra, and R. Borchiellini, “A lattice boltzmann formulation for the analysis of radiative heat transfer problems in a participating medium,” *Numerical Heat Transfer, Part B: Fundamentals*, vol. 57, no. 2, pp. 126–146, Feb. 2010, doi: 10.1080/10407791003613769.

[2] G. R. McNamara, A. L. Garcia, and B. J. Alder, “Stabilization of thermal lattice Boltzmann models,” *J Stat Phys*, vol. 81, no. 1–2, pp. 395–408, Oct. 1995, doi: 10.1007/BF02179986.

[3] X. Shan and X. He, “Discretization of the velocity space in the solution of the boltzmann equation,” *Phys Rev Lett*, 1998, doi: 10.1103/PhysRevLett.80.65.

[4] P. C. Philippi, L. A. Hegele, L. O. E. dos Santos, and R. Surmas, “From the continuous to the lattice Boltzmann equation: The discretization problem and thermal models,” *Phys Rev E Stat Nonlin Soft Matter Phys*, 2006, doi: 10.1103/PhysRevE.73.056702.

[5] X. Shan, X. F. Yuan, and H. Chen, “Kinetic theory representation of hydrodynamics: A way beyond the Navier-Stokes equation,” *J Fluid Mech*, 2006, doi: 10.1017/S0022112005008153.

[6] D. N. Siebert, L. A. Hegele, and P. C. Philippi, “Lattice Boltzmann equation linear stability analysis: Thermal and athermal models,” *Phys Rev E Stat Nonlin Soft Matter Phys*, 2008, doi: 10.1103/PhysRevE.77.026707.

[7] N. Frapolli, S. S. Chikatamarla, and I. v. Karlin, “Multispeed entropic lattice Boltzmann model for thermal flows,” *Phys Rev E Stat Nonlin Soft Matter Phys*, 2014, doi: 10.1103/PhysRevE.90.043306.

[8] I. v. Karlin, D. Sichau, and S. S. Chikatamarla, “Consistent two-population lattice Boltzmann model for thermal flows,” *Phys Rev E Stat Nonlin Soft Matter Phys*, 2013, doi: 10.1103/PhysRevE.88.063310.

[9] F. Klass, A. Gabbana, and A. Bartel, “A non-equilibrium bounce-back boundary condition for thermal multispeed LBM,” *J Comput Sci*, vol. 53, p. 101364, Jul. 2021, doi: 10.1016/J.JOCS.2021.101364.

[10] H. C. Lee, S. Bawazeer, and A. A. Mohamad, “Boundary conditions for lattice Boltzmann method with multispeed lattices,” *Comput Fluids*, vol. 162, 2018, doi: 10.1016/j.compfluid.2017.12.011.

[11] A. Bartoloni *et al.*, “LBE Simulations of Rayleigh-Benard Convection on the APE100 Parallel Processor,” *International Journal of Modern Physics C*, 1993, doi: 10.1142/s012918319300077x.

[12] X. He, S. Chen, and G. D. Doolen, “A Novel Thermal Model for the Lattice Boltzmann Method in Incompressible Limit,” *J Comput Phys*, 1998, doi: 10.1006/jcph.1998.6057.

[13] Z. Guo, C. Zheng, B. Shi, and T. S. Zhao, “Thermal lattice Boltzmann equation for low Mach number flows: Decoupling model,” *Phys Rev E Stat Nonlin Soft Matter Phys*, 2007, doi: 10.1103/PhysRevE.75.036704.

[14] Z. Guo and S. Chang, *Lattice Boltzmann Method and its Applications in Engineering*. 2013.

[15] M. H. Saadat, F. Bösch, and I. V. Karlin, “Lattice Boltzmann model for compressible flows on standard lattices: Variable Prandtl number and adiabatic exponent,” *Phys Rev E*, vol. 99, no. 1, p. 013306, Jan. 2019, doi: 10.1103/PhysRevE.99.013306.

[16] S. C. Mishra and H. K. Roy, “Solving transient conduction and radiation heat transfer problems using the lattice Boltzmann method and the finite volume method,” *J Comput Phys*, vol. 223, no. 1, pp. 89–107, Apr. 2007, doi: 10.1016/J.JCP.2006.08.021.

[17] B. Mondal and S. C. Mishra, “Application of the lattice Boltzmann method and the discrete ordinates method for solving transient conduction and

radiation heat transfer problems,” *Numeri Heat Transf A Appl*, vol. 52, no. 8, pp. 757–775, Jan. 2007, doi: 10.1080/10407780701347663.

[18] S. C. Mishra, A. Lankadasu, and K. N. Beronov, “Application of the lattice Boltzmann method for solving the energy equation of a 2-D transient conduction-radiation problem,” *Int J Heat Mass Transf*, 2005, doi: 10.1016/j.ijheatmasstransfer.2004.10.041.

[19] B. Mondal and X. Li, “Effect of volumetric radiation on natural convection in a square cavity using lattice Boltzmann method with non-uniform lattices,” *Int J Heat Mass Transf*, vol. 53, no. 21–22, pp. 4935–4948, Oct. 2010, doi: 10.1016/J.IJHEATMASSTRANSFER.2010.05.052.

[20] S. C. Mishra, H. Poonia, R. R. Vernekar, and A. K. Das, “Lattice boltzmann method applied to radiative transport analysis in a planar participating medium,” in *Heat Transfer Engineering*, 2014, vol. 35, no. 14–15, pp. 1267–1278, doi: 10.1080/01457632.2013.876806.

[21] S. C. Mishra, H. Poonia, A. K. Das, P. Asinari, and R. Borchiellini, “Analysis of conduction-radiation heat transfer in a 2D enclosure using the lattice boltzmann method,” *Numeri Heat Transf A Appl*, 2014, doi: 10.1080/10407782.2014.894376.

[22] M. Hussain and W. Q. Tao, “Numerical prediction of effective thermal conductivity of ceramic fiber board using lattice Boltzmann method,” *Numeri Heat Transf A Appl*, vol. 74, no. 6, pp. 1285–1300, Sep. 2018, doi: 10.1080/10407782.2018.1523599.

[23] S. Nataraj, K. S. Reddy, and S. P. Thampi, “Lattice Boltzmann simulations of a radiatively participating fluid in Rayleigh–Benard convection,” *Numeri Heat Transf A Appl*, vol. 72, no. 4, pp. 313–329, Aug. 2017, doi: 10.1080/10407782.2017.1376936.

[24] H. A. Tighchi, M. Sobhani, and J. A. Esfahani, “Effect of volumetric radiation on natural convection in a cavity with a horizontal fin using the lattice

Boltzmann method,” *Eur Phys J Plus*, vol. 133, no. 1, Jan. 2018, doi: 10.1140/epjp/i2018-11835-1.

[25] M. Sobhani, H. A. Tighchi, and J. A. Esfahani, “Taguchi optimization of combined radiation/natural convection of participating medium in a cavity with a horizontal fin using LBM,” *Physica A: Statistical Mechanics and its Applications*, vol. 509, pp. 1062–1079, Nov. 2018, doi: 10.1016/j.physa.2018.06.056.

[26] H. Ahmadi Tighchi and J. A. Esfahani, “Combined Radiation/Natural Convection in a Participating Medium Using Novel Lattice Boltzmann Method,” *J Thermophys Heat Trans*, vol. 31, no. 3, pp. 563–574, 2017.

[27] R. McCulloch and H. Bindra, “Coupled radiative and conjugate heat transfer in participating media using lattice Boltzmann methods,” *Comput Fluids*, vol. 124, pp. 261–269, Jan. 2016, doi: 10.1016/j.compfluid.2015.05.024.

[28] M. Lakhi, A. Safavinejad, and M. Lakhi mlakhi, “Numerical investigation of combined force convective-radiative heat transfer in a horizontal channel with lattice Boltzmann method,” vol. 146, pp. 1911–1922, 2021, doi: 10.1007/s10973-020-10136-9.

[29] J. R. Howell, M. P. Mengüç, and R. Siegel, *Thermal radiation heat transfer, sixth edition*. 2015.

[30] M. C. Sukop and D. T. Thorne, *Lattice Boltzmann Modeling*. Berlin Heidelberg : Springer-Verlag , 2006.

[31] S. Succi, *The lattice Boltzmann equation: for fluid dynamics and beyond.* . Oxford University Press, 2001.

[32] P. L. Bhatnagar, E. P. Gross, and M. Krook, “A Model for Collision Processes in Gases. I. Small Amplitude Processes in Charged and Neutral One-Component Systems,” *Physical Review*, vol. 94, no. 3, pp. 511–525, May 1954, doi: 10.1103/PhysRev.94.511.

[33] E. M. Krüger, T., Kusumaatmaja, H., Kuzmin, A., Shardt, O., Silva, G., Viggen, *The Lattice Boltzmann Method*. 2017.

[34] A. Satoh, *Introduction to practice of molecular simulation: molecular dynamics, Monte Carlo, Brownian dynamics, Lattice Boltzmann and dissipative particle dynamics.* . Elsevier, 2010.

[35] F. J. Alexander, S. Chen, and J. D. Sterling, "Lattice Boltzmann thermohydrodynamics," *Phys Rev E*, vol. 47, no. 4, pp. R2249–R2252, Apr. 1993, doi: 10.1103/PhysRevE.47.R2249.

[36] Y. Chen, H. Ohashi, and M. Akiyama, "Thermal lattice Bhatnagar-Gross-Krook model without nonlinear deviations in macrodynamic equations," *Phys Rev E*, vol. 50, no. 4, pp. 2776–2783, Oct. 1994, doi: 10.1103/PhysRevE.50.2776.

[37] L. Biferale *et al.*, "An optimized D2Q37 Lattice Boltzmann code on GP-GPUs," *Comput Fluids*, vol. 80, no. 1, pp. 55–62, Jul. 2013, doi: 10.1016/J.COMPFLUID.2012.06.003.

[38] X. Nie, X. Shan, and H. Chen, "Thermal lattice Boltzmann model for gases with internal degrees of freedom," *Phys Rev E*, vol. 77, no. 3, p. 035701, Mar. 2008, doi: 10.1103/PhysRevE.77.035701.

[39] Grad H., "Approximation to the Boltzmann Equation by Moments," New York, 1948.

[40] A. F. di Rienzo, "Mesoscopic numerical methods for reactive flows: lattice Boltzmann method and beyond," 2012.

[41] M. S. Christopher and B. Mchardy, "A Lattice Boltzmann Method for the Simulation of Light Transfer in Turbid Media and its Application in Computational Studies on Microalgae Growth Kinetics vorgelegt von," 2019.

[42] T. Seta, “Implicit temperature-correction-based immersed-boundary thermal lattice Boltzmann method for the simulation of natural convection,” *Phys Rev E*, vol. 87, no. 6, p. 063304, Jun. 2013, doi: 10.1103/PhysRevE.87.063304.

[43] M. H. Saadat and I. v. Karlin, “Arbitrary Lagrangian–Eulerian formulation of lattice Boltzmann model for compressible flows on unstructured moving meshes,” *Physics of Fluids*, vol. 32, no. 4, p. 046105, Apr. 2020, doi: 10.1063/5.0004024.

[44] Kakaç S., Y. , Yener, and Pramuanjaroenkij A., *Convective Heat Transfer*, 3rd ed. Taylor and Francis Group, 2014.

[45] F. P. Incropera, D. P. Dewitt, T. L. Bergman, and A. S. Lavine, *Principles of Heat and Mass Transfer*, 7th ed. John Wiley and Sons, 2013.

[46] N. I. Prasianakis and I. v. Karlin, “Lattice Boltzmann method for thermal flow simulation on standard lattices,” *Phys Rev E*, vol. 76, no. 1, p. 016702, Jul. 2007, doi: 10.1103/PhysRevE.76.016702.

APPENDICES

A. Equilibrium Distribution Function for Mass and Momentum

Entropic LBM depends on the minimization of entropy function under specific constraints. Solution procedure of the entropy minimization ends up with following equilibrium distribution functions f_i^{eq} for the lattice configuration D2Q9 [46] :

$$f_1^{eq} = \rho(T + u_x^2 - 1)(T + u_y^2 - 1) \tag{A1}$$

$$f_2^{eq} = \frac{\rho}{2}(T + u_x + u_x^2)(1 - T - u_y^2) \tag{A2}$$

$$f_3^{eq} = \frac{\rho}{2}(1 - T - u_x^2)(T + u_y + u_y^2) \tag{A3}$$

$$f_4^{eq} = \frac{\rho}{2}(T - u_x + u_x^2)(1 - T - u_y^2) \tag{A4}$$

$$f_5^{eq} = \frac{\rho}{2}(1 - T - u_x^2)(T - u_y + u_y^2) \tag{A5}$$

$$f_6^{eq} = \frac{\rho}{4}(T + u_x + u_x^2)(T + u_y + u_y^2) \tag{A6}$$

$$f_7^{eq} = \frac{\rho}{4}(T - u_x + u_x^2)(T + u_y + u_y^2) \tag{A7}$$

$$f_8^{eq} = \frac{\rho}{4}(T - u_x + u_x^2)(T - u_y + u_y^2) \tag{A8}$$

$$f_9^{eq} = \frac{\rho}{4}(T + u_x + u_x^2)(T - u_y + u_y^2) \tag{A9}$$

B. The Code for Thermal Model

```
function f=DDFD2Q9_Onsite_Duct()
tic
% clc,clear
close all

%1. GEOMETRY & LATTICE SECTION
Lx=800;
Ly=100;
dx=1;
dy=dx;
x=0:dx:Lx;
y=0:dy:Ly;

[~,n]=size(x);
[~,m]=size(y);
% %Lattice Structure
L=9; %number of Lattices

%2. SOLUTION PARAMETERS SECTION

% dt=dy;
dt=dx;
v=0.04;
diffusivity=0.04;

d=2;
Cv=1;
Cp=Cv;

uynorth=0.0;
uxnorth=0.0;
uysouth=0.0;
uxsouth=0.0;
uywest=0.0;
uxwest=0.04;
    T0=1./3;

Tnorth=1;
Tsouth=1;
Twest=0.333;

mstep2=15000;
```

```
[rho_eq,Absorptivity]=AsinariIntegratedD2Q8(Lx,Ly,mstep
2,Twest,Tnorth,Tsouth);

mstep=65000;
cx=[0 1 0 -1 0 +1 -1 -1 +1 ];
cy=[0 0 1 0 -1 +1 +1 -1 -1 ];


%3. SOLVER SECTION
%3.1 initial values
uxinitial(1:n,1:m)=0;
uyinitial(1:n,1:m)=0;
rhoinitial(1:n,1:m)=1;
Tinitial(1:n,1:m)=1./3;

rho=zeros(n,m)+rhoinitial(1:n,1:m);
ux=zeros(n,m)+uxinitial(1:n,1:m);
uy=zeros(n,m)+uyinitial(1:n,1:m);
T=zeros(n,m)+Tinitial(1:n,1:m);

f=zeros(L,n,m);
g=zeros(L,n,m);

    Tau(1:n,1:m)   = v./T0+dt.*0.5;

omega(1:n,1:m) = 1./Tau(1:n,1:m);
omegaa(1,1:n,1:m)=omega(1:n,1:m);
omegaa(2,1:n,1:m)=omega(1:n,1:m);
omegaa(3,1:n,1:m)=omega(1:n,1:m);
omegaa(4,1:n,1:m)=omega(1:n,1:m);
omegaa(5,1:n,1:m)=omega(1:n,1:m);
omegaa(6,1:n,1:m)=omega(1:n,1:m);
omegaa(7,1:n,1:m)=omega(1:n,1:m);
omegaa(8,1:n,1:m)=omega(1:n,1:m);
omegaa(9,1:n,1:m)=omega(1:n,1:m);

    Tau2(1:n,1:m)  = diffusivity./T0+0.5.*dt;

omega2(1:n,1:m) = 1./Tau2(1:n,1:m);
omegaa2(1,1:n,1:m)=omega2(1:n,1:m);
omegaa2(2,1:n,1:m)=omega2(1:n,1:m);
omegaa2(3,1:n,1:m)=omega2(1:n,1:m);
omegaa2(4,1:n,1:m)=omega2(1:n,1:m);
omegaa2(5,1:n,1:m)=omega2(1:n,1:m);
omegaa2(6,1:n,1:m)=omega2(1:n,1:m);
omegaa2(7,1:n,1:m)=omega2(1:n,1:m);
```

```
omegaa2(8,1:n,1:m)=omega2(1:n,1:m);
omegaa2(9,1:n,1:m)=omega2(1:n,1:m);

w1(1:n,1:m)=1-2.*T0+T0.*T0;
w2(1:n,1:m)=T0./2-T0.*T0./2;
w3(1:n,1:m)=w2(1:n,1:m);
w4(1:n,1:m)=w2(1:n,1:m);
w5(1:n,1:m)=w2(1:n,1:m);
w6(1:n,1:m)=T0.*T0./4;
w7(1:n,1:m)=w6(1:n,1:m);
w8(1:n,1:m)=w6(1:n,1:m);
w9(1:n,1:m)=w6(1:n,1:m);

%3.2 collision process

for t=1:dt:mstep


      if t==1
            rho(1:n,1:m)=rhoinitial(1:n,1:m);

      else
            rho(1:n,1:m)=sum(f(:,1:n,1:m));
      end



M1(1:n,1:m)=cx(1).*f(1,1:n,1:m)+cx(2).*f(2,1:n,1:m)+cx(
3).*f(3,1:n,1:m)+cx(4).*f(4,1:n,1:m)+cx(5).*f(5,1:n,1:m
)+cx(6).*f(6,1:n,1:m)+...

+cx(7).*f(7,1:n,1:m)+cx(8).*f(8,1:n,1:m)+cx(9).*f(9,1:n
,1:m);


M2(1:n,1:m)=cy(1).*f(1,1:n,1:m)+cy(2).*f(2,1:n,1:m)+cy(
3).*f(3,1:n,1:m)+cy(4).*f(4,1:n,1:m)+cy(5).*f(5,1:n,1:m
)+cy(6).*f(6,1:n,1:m)+...

+cy(7).*f(7,1:n,1:m)+cy(8).*f(8,1:n,1:m)+cy(9).*f(9,1:n
,1:m);

if t==1
            ux(1:n,1:m)=uxinitial;
            uy(1:n,1:m)=uyinitial;
```

```
else
            ux(1:n,1:m)=M1(1:n,1:m)./rho(1:n,1:m);
            uy(1:n,1:m)=M2(1:n,1:m)./rho(1:n,1:m);
end
ux(n,:)=(4.*ux(n-1,:)-ux(n-2,:))./3;

M3(1:n,1:m)=g(1,1:n,1:m)+g(2,1:n,1:m)+g(3,1:n,1:m)+g(4,
1:n,1:m)+g(5,1:n,1:m)+...

g(6,1:n,1:m)+g(7,1:n,1:m)+g(8,1:n,1:m)+g(9,1:n,1:m);

coeff3(1:n,1:m)=(sqrt(ux(1:n,1:m).*ux(1:n,1:m)+uy(1:n,1
:m).*uy(1:n,1:m))).^2;

if t==1
    T(1:n,1:m)=Tinitial(1:n,1:m);
else
T(1:n,1:m)=(M3(1:n,1:m)./rho(1:n,1:m)+0.5.*Qa(1:n,1:m).
/rho(1:n,1:m)-coeff3(1:n,1:m))./(d.*Cv);
end

E(1:n,1:m)=Cv.*T(1:n,1:m)+0.5.*(coeff3(1:n,1:m));

h=zeros(L,n,m);
feq=zeros(L,n,m);
geq=zeros(L,n,m);


h(1,1:n,1:m)=(T0+ux(1:n,1:m).*ux(1:n,1:m)-
1).*(T0+uy(1:n,1:m).*uy(1:n,1:m)-1);

h(2,1:n,1:m)=(T0+ux(1:n,1:m)+ux(1:n,1:m).*ux(1:n,1:m)).
*(1-T0-uy(1:n,1:m).*uy(1:n,1:m));
                h(3,1:n,1:m)=(1-T0-
ux(1:n,1:m).*ux(1:n,1:m)).*(T0+uy(1:n,1:m)+uy(1:n,1:m).
*uy(1:n,1:m));
                h(4,1:n,1:m)=(T0-
ux(1:n,1:m)+ux(1:n,1:m).*ux(1:n,1:m)).*(1-T0-
uy(1:n,1:m).*uy(1:n,1:m));
                h(5,1:n,1:m)=(1-T0-
ux(1:n,1:m).*ux(1:n,1:m)).*(T0-
uy(1:n,1:m)+uy(1:n,1:m).*uy(1:n,1:m));
h(6,1:n,1:m)=(T0+ux(1:n,1:m)+ux(1:n,1:m).*ux(1:n,1:m)).
*(T0+uy(1:n,1:m)+uy(1:n,1:m).*uy(1:n,1:m));
```

```
                h(7,1:n,1:m)=(T0-
ux(1:n,1:m)+ux(1:n,1:m).*ux(1:n,1:m)).*(T0+uy(1:n,1:m)+
uy(1:n,1:m).*uy(1:n,1:m));
                h(8,1:n,1:m)=(T0-
ux(1:n,1:m)+ux(1:n,1:m).*ux(1:n,1:m)).*(T0-
uy(1:n,1:m)+uy(1:n,1:m).*uy(1:n,1:m));

h(9,1:n,1:m)=(T0+ux(1:n,1:m)+ux(1:n,1:m).*ux(1:n,1:m)).
*(T0-uy(1:n,1:m)+uy(1:n,1:m).*uy(1:n,1:m));

H1(1:n,1:m)   =h(1,1:n,1:m);
H2(1:n,1:m)   =h(2,1:n,1:m);
H3(1:n,1:m)   =h(3,1:n,1:m);
H4(1:n,1:m)   =h(4,1:n,1:m);
H5(1:n,1:m)   =h(5,1:n,1:m);
H6(1:n,1:m)   =h(6,1:n,1:m);
H7(1:n,1:m)   =h(7,1:n,1:m);
H8(1:n,1:m)   =h(8,1:n,1:m);
H9(1:n,1:m)   =h(9,1:n,1:m);


feq(1,1:n,1:m)=rho(1:n,1:m).*H1(1:n,1:m);

feq(2,1:n,1:m)=0.5.*rho(1:n,1:m).*H2(1:n,1:m);

feq(3,1:n,1:m)=0.5.*rho(1:n,1:m).*H3(1:n,1:m);

feq(4,1:n,1:m)=0.5.*rho(1:n,1:m).*H4(1:n,1:m);

feq(5,1:n,1:m)=0.5.*rho(1:n,1:m).*H5(1:n,1:m);

feq(6,1:n,1:m)=0.25.*rho(1:n,1:m).*H6(1:n,1:m);

feq(7,1:n,1:m)=0.25.*rho(1:n,1:m).*H7(1:n,1:m);

feq(8,1:n,1:m)=0.25.*rho(1:n,1:m).*H8(1:n,1:m);

feq(9,1:n,1:m)=0.25.*rho(1:n,1:m).*H9(1:n,1:m);

c2=cx.*cx+cy.*cy;

qx(1:n,1:m)=rho(1:n,1:m).*ux(1:n,1:m).*(d.*T(1:n,1:m)+c
oeff3(1:n,1:m))+2.*rho(1:n,1:m).*T0.*ux(1:n,1:m);
qy(1:n,1:m)=rho(1:n,1:m).*uy(1:n,1:m).*(d.*T(1:n,1:m)+c
oeff3(1:n,1:m))+2.*rho(1:n,1:m).*T0.*uy(1:n,1:m);
```

```
Rxx(1:n,1:m)=rho(1:n,1:m).*(d.*T(1:n,1:m)+coeff3(1:n,1:
m)).*(T0+ux(1:n,1:m).*ux(1:n,1:m))...

+2.*rho(1:n,1:m).*T0.*(T0+2.*ux(1:n,1:m).*ux(1:n,1:m));


Rxy(1:n,1:m)=rho(1:n,1:m).*(d.*T(1:n,1:m)+coeff3(1:n,1:
m)).*(ux(1:n,1:m).*uy(1:n,1:m))...

+2.*rho(1:n,1:m).*T0.*(2.*ux(1:n,1:m).*uy(1:n,1:m));


Ryy(1:n,1:m)=rho(1:n,1:m).*(d.*T(1:n,1:m)+coeff3(1:n,1:
m)).*(T0+uy(1:n,1:m).*uy(1:n,1:m))...

+2.*rho(1:n,1:m).*T0.*(T0+2.*uy(1:n,1:m).*uy(1:n,1:m));


geq(1,1:n,1:m)=w1(1:n,1:m).*(2.*rho(1:n,1:m).*E(1:n,1:m
)+qx(1:n,1:m).*cx(1)./T0+qy(1:n,1:m).*cy(1)./T0...

+(Rxx(1:n,1:m).*cx(1).*cx(1)+2.*Rxy(1:n,1:m).*cx(1).*cy
(1)+Ryy(1:n,1:m).*cy(1).*cy(1))./(2.*T0.*T0)...
                                                -
(Rxx(1:n,1:m).*T0+Ryy(1:n,1:m).*T0)./(2.*T0.*T0)...
                                                -
(2.*rho(1:n,1:m).*E(1:n,1:m).*T0.*c2(1))./(2.*T0.*T0)..
.

+(2.*rho(1:n,1:m).*E(1:n,1:m)));

geq(2,1:n,1:m)=w2(1:n,1:m).*(2.*rho(1:n,1:m).*E(1:n,1:m
)+qx(1:n,1:m).*cx(2)./T0+qy(1:n,1:m).*cy(2)./T0...

+(Rxx(1:n,1:m).*cx(2).*cx(2)+2.*Rxy(1:n,1:m).*cx(2).*cy
(2)+Ryy(1:n,1:m).*cy(2).*cy(2))./(2.*T0.*T0)...
                                                -
(Rxx(1:n,1:m).*T0+Ryy(1:n,1:m).*T0)./(2.*T0.*T0)...
                                                -
(2.*rho(1:n,1:m).*E(1:n,1:m).*T0.*c2(2))./(2.*T0.*T0)..
.

+(2.*rho(1:n,1:m).*E(1:n,1:m)));
```

```
geq(3,1:n,1:m)=w3(1:n,1:m).*(2.*rho(1:n,1:m).*E(1:n,1:m
)+qx(1:n,1:m).*cx(3)./T0+qy(1:n,1:m).*cy(3)./T0...

+(Rxx(1:n,1:m).*cx(3).*cx(3)+2.*Rxy(1:n,1:m).*cx(3).*cy
(3)+Ryy(1:n,1:m).*cy(3).*cy(3))./(2.*T0.*T0)...
                                                -
(Rxx(1:n,1:m).*T0+Ryy(1:n,1:m).*T0)./(2.*T0.*T0)...
                                                -
(2.*rho(1:n,1:m).*E(1:n,1:m).*T0.*c2(3))./(2.*T0.*T0)..
.

+(2.*rho(1:n,1:m).*E(1:n,1:m)));

geq(4,1:n,1:m)=w4(1:n,1:m).*(2.*rho(1:n,1:m).*E(1:n,1:m
)+qx(1:n,1:m).*cx(4)./T0+qy(1:n,1:m).*cy(4)./T0...

+(Rxx(1:n,1:m).*cx(4).*cx(4)+2.*Rxy(1:n,1:m).*cx(4).*cy
(4)+Ryy(1:n,1:m).*cy(4).*cy(4))./(2.*T0.*T0)...
                                                -
(Rxx(1:n,1:m).*T0+Ryy(1:n,1:m).*T0)./(2.*T0.*T0)...
                                                -
(2.*rho(1:n,1:m).*E(1:n,1:m).*T0.*c2(4))./(2.*T0.*T0)..
.

+(2.*rho(1:n,1:m).*E(1:n,1:m)));

geq(5,1:n,1:m)=w5(1:n,1:m).*(2.*rho(1:n,1:m).*E(1:n,1:m
)+qx(1:n,1:m).*cx(5)./T0+qy(1:n,1:m).*cy(5)./T0...

+(Rxx(1:n,1:m).*cx(5).*cx(5)+2.*Rxy(1:n,1:m).*cx(5).*cy
(5)+Ryy(1:n,1:m).*cy(5).*cy(5))./(2.*T0.*T0)...
                                                -
(Rxx(1:n,1:m).*T0+Ryy(1:n,1:m).*T0)./(2.*T0.*T0)...
                                                -
(2.*rho(1:n,1:m).*E(1:n,1:m).*T0.*c2(5))./(2.*T0.*T0)..
.

+(2.*rho(1:n,1:m).*E(1:n,1:m)));

geq(6,1:n,1:m)=w6(1:n,1:m).*(2.*rho(1:n,1:m).*E(1:n,1:m
)+qx(1:n,1:m).*cx(6)./T0+qy(1:n,1:m).*cy(6)./T0...

+(Rxx(1:n,1:m).*cx(6).*cx(6)+2.*Rxy(1:n,1:m).*cx(6).*cy
(6)+Ryy(1:n,1:m).*cy(6).*cy(6))./(2.*T0.*T0)...
```

```
-
(Rxx(1:n,1:m).*T0+Ryy(1:n,1:m).*T0)./(2.*T0.*T0)...
-
(2.*rho(1:n,1:m).*E(1:n,1:m).*T0.*c2(6))./(2.*T0.*T0)..
.

+(2.*rho(1:n,1:m).*E(1:n,1:m)));

geq(7,1:n,1:m)=w7(1:n,1:m).*(2.*rho(1:n,1:m).*E(1:n,1:m
)+qx(1:n,1:m).*cx(7)./T0+qy(1:n,1:m).*cy(7)./T0...

+(Rxx(1:n,1:m).*cx(7).*cx(7)+2.*Rxy(1:n,1:m).*cx(7).*cy
(7)+Ryy(1:n,1:m).*cy(7).*cy(7))./(2.*T0.*T0)...
-
(Rxx(1:n,1:m).*T0+Ryy(1:n,1:m).*T0)./(2.*T0.*T0)...
-
(2.*rho(1:n,1:m).*E(1:n,1:m).*T0.*c2(7))./(2.*T0.*T0)..
.

+(2.*rho(1:n,1:m).*E(1:n,1:m)));

geq(8,1:n,1:m)=w8(1:n,1:m).*(2.*rho(1:n,1:m).*E(1:n,1:m
)+qx(1:n,1:m).*cx(8)./T0+qy(1:n,1:m).*cy(8)./T0...

+(Rxx(1:n,1:m).*cx(8).*cx(8)+2.*Rxy(1:n,1:m).*cx(8).*cy
(8)+Ryy(1:n,1:m).*cy(8).*cy(8))./(2.*T0.*T0)...
-
(Rxx(1:n,1:m).*T0+Ryy(1:n,1:m).*T0)./(2.*T0.*T0)...
-
(2.*rho(1:n,1:m).*E(1:n,1:m).*T0.*c2(8))./(2.*T0.*T0)..
.

+(2.*rho(1:n,1:m).*E(1:n,1:m)));

geq(9,1:n,1:m)=w9(1:n,1:m).*(2.*rho(1:n,1:m).*E(1:n,1:m
)+qx(1:n,1:m).*cx(9)./T0+qy(1:n,1:m).*cy(9)./T0...

+(Rxx(1:n,1:m).*cx(9).*cx(9)+2.*Rxy(1:n,1:m).*cx(9).*cy
(9)+Ryy(1:n,1:m).*cy(9).*cy(9))./(2.*T0.*T0)...
-
(Rxx(1:n,1:m).*T0+Ryy(1:n,1:m).*T0)./(2.*T0.*T0)...
-
(2.*rho(1:n,1:m).*E(1:n,1:m).*T0.*c2(9))./(2.*T0.*T0)..
.

+(2.*rho(1:n,1:m).*E(1:n,1:m)));
```

```
StefanBoltzmann=1;
Constant1(1:L,1:n,1:m)=1.0-0.5.*omegaa(1:L,1:n,1:m);

Qb(1:n,1:m)=(4.*(Absorptivity).*StefanBoltzmann.*(T(1:n
,1:m)).^4-(Absorptivity).*rho_eq(1:n,1:m));

      C2=1;
      beta=1;
      alfa=diffusivity;
      conductivity=diffusivity;
      Tref=Tsouth;
      N=beta.*conductivity./4./Tref.^3;
      C3=beta.*alfa./4./N;

            Qa(1:n,1:m)=-
C2.*C3.*Qb(1:n,1:m).*rho(1:n,1:m).*2./Ly.^2;
            Q(1:n,1:m)=-
C2.*C3.*Qb(1:n,1:m).*rho(1:n,1:m).*2./Ly.^2;

   Q1(1:n,1:m)=w1.*Q(1:n,1:m);
   Q2(1:n,1:m)=w2.*Q(1:n,1:m);
   Q3(1:n,1:m)=w3.*Q(1:n,1:m);
   Q4(1:n,1:m)=w4.*Q(1:n,1:m);
   Q5(1:n,1:m)=w5.*Q(1:n,1:m);
   Q6(1:n,1:m)=w6.*Q(1:n,1:m);
   Q7(1:n,1:m)=w7.*Q(1:n,1:m);
   Q8(1:n,1:m)=w8.*Q(1:n,1:m);
   Q9(1:n,1:m)=w9.*Q(1:n,1:m);

   q(1,1:n,1:m)=Q1(1:n,1:m);
   q(2,1:n,1:m)=Q2(1:n,1:m);
   q(3,1:n,1:m)=Q3(1:n,1:m);
   q(4,1:n,1:m)=Q4(1:n,1:m);
   q(5,1:n,1:m)=Q5(1:n,1:m);
   q(6,1:n,1:m)=Q6(1:n,1:m);
   q(7,1:n,1:m)=Q7(1:n,1:m);
   q(8,1:n,1:m)=Q8(1:n,1:m);
   q(9,1:n,1:m)=Q9(1:n,1:m);


f(1:L,1:n,1:m)=dt.*omegaa(1:L,1:n,1:m).*feq(1:L,1:n,1:m
)+(1-dt.*omegaa(1:L,1:n,1:m)).*f(1:L,1:n,1:m);
```

```
g(1:L,1:n,1:m)=dt.*omegaa(1:L,1:n,1:m).*geq(1:L,1:n,1:m
)+(1-dt.*omegaa(1:L,1:n,1:m)).*g(1:L,1:n,1:m)+ ...

+Constant1(1:L,1:n,1:m).*dt.*q(1:L,1:n,1:m);

%3.3 streaming process
        f(1,1:n,1:m)=f(1,1:n,1:m);
        g(1,1:n,1:m)=g(1,1:n,1:m);

        f(2,n:-1:2,1:m)=f(2,n-1:-1:1,1:m);
        g(2,n:-1:2,1:m)=g(2,n-1:-1:1,1:m);

        f(3,1:n,m:-1:2)=f(3,1:n,m-1:-1:1);
        g(3,1:n,m:-1:2)=g(3,1:n,m-1:-1:1);

        f(4,1:n-1,1:m)=f(4,2:n,1:m);
        g(4,1:n-1,1:m)=g(4,2:n,1:m);

        f(5,1:n,1:m-1)=f(5,1:n,2:m);
        g(5,1:n,1:m-1)=g(5,1:n,2:m);

        f(6,n:-1:2,m:-1:2)=f(6,n-1:-1:1,m-1:-1:1);
        g(6,n:-1:2,m:-1:2)=g(6,n-1:-1:1,m-1:-1:1);

        f(7,1:n-1,m:-1:2)=f(7,2:n,m-1:-1:1);
        g(7,1:n-1,m:-1:2)=g(7,2:n,m-1:-1:1);

        f(8,1:n-1,1:m-1)=f(8,2:n,2:m);
        g(8,1:n-1,1:m-1)=g(8,2:n,2:m);

        f(9,n:-1:2,1:m-1)=f(9,n-1:-1:1,2:m);
        g(9,n:-1:2,1:m-1)=g(9,n-1:-1:1,2:m);

%3.4 Boundary Conditions

for i=1:n

%top (north), y=100, Dirichlet
rho(i,m)=(1./(1+uynorth)).*(f(1,i,m)+f(2,i,m)+f(4,i,m)+
2.*f(3,i,m)+2.*f(6,i,m)+2.*f(7,i,m));
f(9,i,m)=0.5.*rho(i,m).*(uxnorth-uynorth)+0.5.*(-
f(2,i,m)+f(4,i,m)+2.*f(7,i,m)-feq(5,i,m)+feq(3,i,m));
f(5,i,m)=feq(5,i,m)+f(3,i,m)-feq(3,i,m);
f(8,i,m)=-rho(i,m).*uynorth+f(3,i,m)+f(6,i,m)+f(7,i,m)-
f(5,i,m)-f(9,i,m);
```

```
E(i,m)=(Cv.*Tnorth+0.5.*coeff3(i,m)).*2.*rho(i,m)-
0.5*Qa(i,m);

g(9,i,m)=geq(9,i,m)+geq(7,i,m)-g(7,i,m);
g(5,i,m)=geq(5,i,m)+geq(3,i,m)-g(3,i,m);
g(8,i,m)=geq(8,i,m)+geq(6,i,m)-g(6,i,m);

%bottom (south), y=0, Dirichlet
rho(i,1)=(1./(1-
uysouth)).*(f(1,i,1)+f(2,i,1)+f(4,i,1)+2.*f(5,i,1)+2.*f
(8,i,1)+2.*f(9,i,1));
f(6,i,1)=0.5.*rho(i,1).*(uxsouth+uysouth)+0.5.*(-
f(2,i,1)+f(4,i,1)+2.*f(8,i,1)+feq(5,i,1)-feq(3,i,1));
f(3,i,1)=feq(3,i,1)+f(5,i,1)-feq(5,i,1);
f(7,i,1)=rho(i,1).*uysouth-f(3,i,1)-
f(6,i,1)+f(5,i,1)+f(8,i,1)+f(9,i,1);

E(i,1)=(Cv.*Tsouth+0.5.*coeff3(i,1)).*2.*rho(i,1)-
0.5*Qa(i,1);

g(6,i,1)=geq(6,i,1)+geq(8,i,1)-g(8,i,1);
g(3,i,1)=geq(3,i,1)+geq(5,i,1)-g(5,i,1);
g(7,i,1)=geq(7,i,1)+geq(9,i,1)-g(9,i,1);
end

for j=1:m

    %left (west), x=0, Dirichlet
rho(1,j)=(1./(1-
uxwest)).*(f(1,1,j)+f(3,1,j)+f(5,1,j)+2.*f(4,1,j)+2.*f(
7,1,j)+2.*f(8,1,j));
f(6,1,j)=0.5.*rho(1,j).*(uxwest+uywest)+0.5.*(-
feq(2,1,j)+feq(4,1,j)-f(3,1,j)+f(5,1,j)+2.*f(8,1,j));
f(2,1,j)=feq(2,1,j)+f(4,1,j)-feq(4,1,j);
f(9,1,j)=rho(1,j).*uxwest-f(2,1,j)-
f(6,1,j)+f(7,1,j)+f(4,1,j)+f(8,1,j);

E(1,j)=(Cv.*Twest+0.5.*coeff3(1,j)).*2.*rho(1,j)-
0.5.*Qa(1,j);
g(6,1,j)=geq(6,1,j)+geq(8,1,j)-g(8,1,j);
g(2,1,j)=geq(2,1,j)+geq(4,1,j)-g(4,1,j);
g(9,1,j)=geq(9,1,j)+geq(7,1,j)-g(7,1,j);


    %right (east), x=0, Dirichlet
```

```
%For Duct
rho(n,j)=(1./(1+ux(n,j))).*(f(1,n,j)+f(3,n,j)+f(5,n,j)+
2.*f(2,n,j)+2.*f(6,n,j)+2.*f(9,n,j));
f(8,n,j)=-0.5.*rho(n,j).*(ux(n,j)+uy(n,j))-
0.5.*(feq(4,n,j)-feq(2,n,j)-f(3,n,j)+f(5,n,j)-
2.*f(6,n,j));
f(4,n,j)=feq(4,n,j)+f(2,n,j)-feq(2,n,j);
f(7,n,j)=-(rho(n,j).*ux(n,j)-f(2,n,j)-f(6,n,j)-
f(9,n,j)+f(4,n,j)+f(8,n,j));

% %For Duct
g(4,n,j)=(4.*g(4,n-1,j)-g(4,n-2,j))./3;
g(7,n,j)=(4.*g(7,n-1,j)-g(7,n-2,j))./3;
g(8,n,j)=(4.*g(8,n-1,j)-g(8,n-2,j))./3;

end

    fprintf('time=%g seconds \n',t)
    fprintf('...............\n')


end
```

C. The Code for RTLBM

```
function
[rho_eq,Absorptivity]=AsinariIntegratedD2Q8(Lx,Ly,mstep
,Twest,Tnorth,Tsouth)
% clc,clear
% close all
beta=1;
scattering=0;
Absorptivity=beta-scattering;

%1. GEOMETRY & LATTICE SECTION
R=(Lx)./(Ly);

%boundaries of  geometrical domain
dx=1.*R./Lx;
dy=dx;
x=0:dx:1.*R;
y=0:dy:1;
```

```
[~,n]=size(x);
[~,m]=size(y);

% %Lattice Structure
L=8; %number of Lattices

%2. SOLUTION PARAMETERS SECTION

dt=dy;

%2. SOLUTION PARAMETERS SECTION
U=1;

%2.1 velocity magnitudes

e=[U U U U sqrt(2).*U sqrt(2).*U sqrt(2).*U sqrt(2).*U
];


Tau(1:L)=1./(e(1:L).*beta);
omega(1:L)=dt./Tau(1:L);

StefanBoltzmann=1;
I_wall_south=(StefanBoltzmann.*4).*Tsouth.^4;
I_wall_west=(StefanBoltzmann.*4).*Twest.^4;
I_wall_top=(StefanBoltzmann.*4).*Tnorth.^4;

%weights for integration

w=zeros(1,L)+1./8;

%3. SOLVER SECTION
%3.1 initial values
rho=zeros(n,m);

f(1,1:n,1:m)=w(1).*rho(1:n,1:m);
f(2,1:n,1:m)=w(2).*rho(1:n,1:m);
f(3,1:n,1:m)=w(3).*rho(1:n,1:m);
f(4,1:n,1:m)=w(4).*rho(1:n,1:m);
f(5,1:n,1:m)=w(5).*rho(1:n,1:m);
f(6,1:n,1:m)=w(6).*rho(1:n,1:m);
f(7,1:n,1:m)=w(7).*rho(1:n,1:m);
f(8,1:n,1:m)=w(8).*rho(1:n,1:m);
```

```
%3.2 collision process
for t=1:dt:mstep.*dt


rho(1:n,1:m)=w(1).*f(1,1:n,1:m)+w(2).*f(2,1:n,1:m)+w(3)
.*f(3,1:n,1:m)+w(4).*f(4,1:n,1:m)+w(5).*f(5,1:n,1:m)...

+w(6).*f(6,1:n,1:m)+w(7).*f(7,1:n,1:m)+w(8).*f(8,1:n,1:
m);

               feq(1,1:n,1:m)=rho(1:n,1:m);
               feq(2,1:n,1:m)=rho(1:n,1:m);
               feq(3,1:n,1:m)=rho(1:n,1:m);
               feq(4,1:n,1:m)=rho(1:n,1:m);
               feq(5,1:n,1:m)=rho(1:n,1:m);
               feq(6,1:n,1:m)=rho(1:n,1:m);
               feq(7,1:n,1:m)=rho(1:n,1:m);
               feq(8,1:n,1:m)=rho(1:n,1:m);


f(1,1:n,1:m)=omega(1).*feq(1,1:n,1:m)+(1-
omega(1)).*f(1,1:n,1:m); %pdf

f(2,1:n,1:m)=omega(2).*feq(2,1:n,1:m)+(1-
omega(2)).*f(2,1:n,1:m); %pdf

f(3,1:n,1:m)=omega(3).*feq(3,1:n,1:m)+(1-
omega(3)).*f(3,1:n,1:m); %pdf

f(4,1:n,1:m)=omega(4).*feq(4,1:n,1:m)+(1-
omega(4)).*f(4,1:n,1:m); %pdf

f(5,1:n,1:m)=omega(5).*feq(5,1:n,1:m)+(1-
omega(5)).*f(5,1:n,1:m); %pdf

f(6,1:n,1:m)=omega(6).*feq(6,1:n,1:m)+(1-
omega(6)).*f(6,1:n,1:m); %pdf

f(7,1:n,1:m)=omega(7).*feq(7,1:n,1:m)+(1-
omega(7)).*f(7,1:n,1:m); %pdf

f(8,1:n,1:m)=omega(8).*feq(8,1:n,1:m)+(1-
omega(8)).*f(8,1:n,1:m); %pdf
```

```
rho_eq(1:n,1:m)=w(1).*f(1,1:n,1:m)+w(2).*f(2,1:n,1:m)+w
(3).*f(3,1:n,1:m)+w(4).*f(4,1:n,1:m)+w(5).*f(5,1:n,1:m)
...

+w(6).*f(6,1:n,1:m)+w(7).*f(7,1:n,1:m)+w(8).*f(8,1:n,1:
m);

%3.3 streaming process
        f(1,n:-1:2,1:m)=f(1,n-1:-1:1,1:m);
        f(2,1:n,m:-1:2)=f(2,1:n,m-1:-1:1);
        f(3,1:n-1,1:m)=f(3,2:n,1:m);
        f(4,1:n,1:m-1)=f(4,1:n,2:m);
        f(5,n:-1:2,m:-1:2)=f(5,n-1:-1:1,m-1:-1:1);
        f(6,1:n-1,m:-1:2)=f(6,2:n,m-1:-1:1);
        f(7,1:n-1,1:m-1)=f(7,2:n,2:m);
        f(8,n:-1:2,1:m-1)=f(8,n-1:-1:1,2:m);

%3.4 Boundary Conditions

f(1,1,1:m)    = I_wall_west;
f(5,1,1:m)    = I_wall_west;
f(8,1,1:m)    = I_wall_west;

f(3,n,1:m)    = (4.*f(3,n-1,1:m)-f(3,n-2,1:m))./3;
f(7,n,1:m)    = (4.*f(7,n-1,1:m)-f(7,n-2,1:m))./3;
f(6,n,1:m)    = (4.*f(6,n-1,1:m)-f(6,n-2,1:m))./3;

f(4,1:n,m)   =  I_wall_top;
f(7,1:n,m)   =  I_wall_top;
f(8,1:n,m)   =  I_wall_top;

f(5,1:n,1)   =  I_wall_south;
f(2,1:n,1)   =  I_wall_south;
f(6,1:n,1)   =  I_wall_south;

end


end
```

CURRICULUM VITAE

Surname, Name: Gümüşsu, Emre

EDUCATION

Degree	Institution	Year of Graduation
MS	Hacettepe University Mechanical Engineering	2017
BS	Hacettepe University Mechanical Engineering	2015
High School	Ankara Atatürk High School	2008

FOREIGN LANGUAGES

Advanced English, Upper-intermediate German

PUBLICATIONS

1. Gümüşsu E., Ekici Ö., Köksal M., " 3-D CFD modeling and experimental testing of thermal behavior of a Li-Ion battery ", Applied Thermal Engineering, 120, 484-495 (2017)

2. Gümüşsu E., Tarman I. H., " Multi-Mode Heat Transfer using Total Energy based Entropic Lattice Boltzmann Method ", Fourteenth International Conference on Thermal Engineering: Theory and Applications, 25-27 May 2023, Yalova, Turkey.

3. Gümüşsu E., Tarman I. H., "Numerical Simulation of Duct Flow in the Presence of Participating Media Radiation with Total Energy Based Entropic Lattice Boltzmann Method", International Journal of Thermofluids, **(Under Review)**